JOURNAL OF PETROLOGY | VOLUME 40 | NUMBER 8 | PAGES 1211–1239 | 1999

Petrology of Sapphirine-bearing and Associated Granulites from Central Sri Lanka

LEO M. KRIEGSMAN[1]* AND JOHN C. SCHUMACHER[2]†

[1]INSTITUT FÜR GEOWISSENSCHAFTEN, JOHANNES GUTENBERG UNIVERSITÄT, SAARSTRASSE 21, 55122 MAINZ, GERMANY

[2]INSTITUT FÜR MINERALOGIE, PETROLOGIE UND GEOCHEMIE, ALBERT-LUDWIGS-UNIVERSITÄT, ALBERTSTRASSE 23B, 79104 FREIBURG, GERMANY

RECEIVED AUGUST 10, 1996; REVISED TYPESCRIPT ACCEPTED JANUARY 29, 1999

Calcium-poor, magnesian granulites from two localities in central Sri Lanka contain a rich variety of assemblages composed of combinations of sapphirine (Spr), garnet, orthopyroxene, sillimanite, cordierite or spinel. Quartz is present in some assemblages at the Hakurutale locality, and corundum and rare gedrite are present in some assemblages at the Munwatte locality. Rocks from both localities display diverse sets of inclusion and sequential reaction textures. The inclusions suggest that the earliest assemblage at Munwatte was orthopyroxene + spinel + corundum. Garnet growth followed by garnet breakdown occurred via the reactions orthopyroxene + corundum = garnet and garnet + corundum + spinel = sapphirine. This produced coarse-grained coronas of sapphirine around the corundum and spinel. The earliest assemblage at Hakurutale was orthopyroxene + sillimanite + sapphirine. Garnet growth occurred via the reactions orthopyroxene + sillimanite + sapphirine = garnet and orthopyroxene + sillimanite = garnet + quartz. Locally, garnet was partially destroyed by a variety of corona-forming continuous reactions. The most important are garnet = orthopyroxene + sillimanite + sapphirine and garnet + sillimanite = sapphirine + cordierite (both localities) and, at Hakurutale, garnet + quartz = orthopyroxene + sillimanite, garnet + sillimanite + quartz = cordierite and garnet + quartz = orthopyroxene + cordierite. In places, orthopyroxene + sillimanite + quartz reacted to form cordierite, and orthopyroxene + sillimanite reacted to form cordierite + sapphirine coronas. At Hakurutale, inclusion textures indicate that sapphirine was present in the earliest recorded assemblages (prograde), but also formed later as various corona-forming reactions occurred. On the basis of calculated orientations of model univariant curves and continuous reaction slopes for the observed phases, the P–T *path is roughly a 'clockwise' (i.e.* P_{max} *precedes* T_{max}*) trajectory. The earlier, garnet-forming stage reflects heating possibly with a slight* P *increase. The final recorded leg suggests near-isothermal decompression starting at a peak* P–T *of about 9 kbar and 830°C and dropping to nearly 7·5 kbar at about 810°C. Sapphirine appears to have developed at several points along the* P–T *trajectory.*

KEY WORDS: *granulite; near-isothermal decompression; P–T path; reaction sequence*

INTRODUCTION

Rocks of highly aluminous and magnesian bulk composition commonly record a part of the *P–T* path close to peak temperatures (e.g. Hensen, 1987), where the sense of the *P–T* path—clockwise or counter-clockwise—may be determined. These rocks generally contain a subset of the minerals garnet (Gar), orthopyroxene (Opx), cordierite (Crd), Al-spinel (Sp) and sapphirine (Spr), in combination with sillimanite (Sil), corundum (Cor) or quartz (Qz). They have been increasingly used in the last few years to deduce parts of the *P–T* paths witnessed by granulite-facies terranes (e.g. Droop & Bucher-Nurminen, 1984; Droop, 1989; Bertrand *et al.*, 1992;

*Present address: Department of Geology and Mineralogy, University of Turku, FIN 20014 Turku, Finland.
†Corresponding author. Present address: Department of Earth Sciences, University of Bristol, Bristol BS8 1RJ, UK. Tel: +44 117 954-5417. Fax: +44 117 925-3385. e-mail: j.c.schumacher@bristol.ac.uk

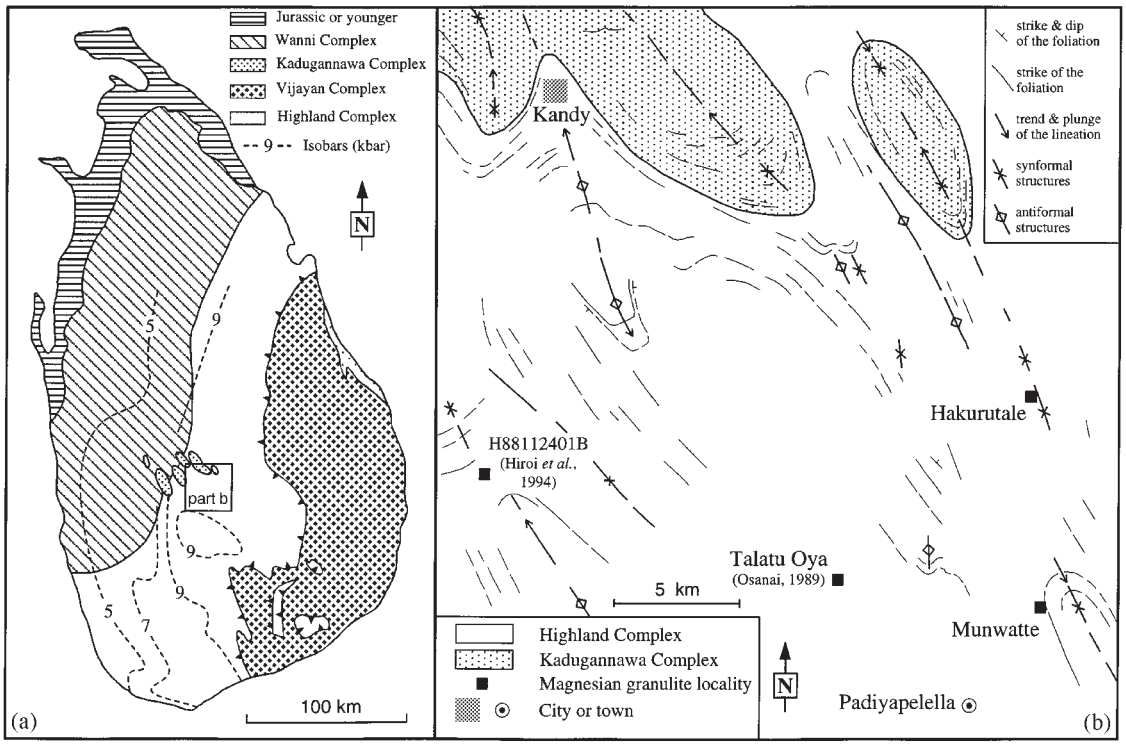

Fig. 1. (a) Subdivision of the Sri Lankan high-grade terrane, as well as isobars (at T>750°C) drawn after data of Schumacher *et al.* (1990), Faulhaber & Raith (1991) and Schumacher & Faulhaber (1994). (b) Simplified map of the Kandy area in central Sri Lanka. Two localities (Hakurutale and Munwatte) with sapphirine-bearing granulites. Osanai (1989) and Hiroi *et al.* (1994) described two other localities in the same area. It should be noted that all four localities are located in the area where P>9 kbar.

Goscombe, 1992). We report similar rocks from central Sri Lanka that display spectacular reaction textures and are highly suitable for petrologic analysis.

The basement gneisses of Sri Lanka have been subdivided into four units [modified after Kröner (1991); Cooray (1994)]: (1) Highland Complex; (2) Vijayan Complex; (3) Kadugannawa Complex; (4) Wanni Complex (Fig. 1). The Highland Complex consists of highly deformed and metamorphosed rocks of sedimentary and igneous parentage. The Nd model ages in this unit are 2–3 Ga, whereas the other units give Nd model ages of 1–2 Ga (Milisenda *et al.*, 1988). Evidence from the U–Pb system strongly suggests that the age of granulite-facies metamorphism is in the range 610–550 Ma (Baur *et al.*, 1991; Hölzl *et al.*, 1994).

Gneisses of the Highland Complex in central Sri Lanka show a well-developed gneissic layering (S_2) and a strong, NNW–SSE oriented mineral and stretching lineation (L_2), defined by peak metamorphic assemblages in all rock types (e.g. Kriegsman, 1994). Compositional banding is generally parallel to S_2. Together, they have been refolded around upright folds with gently plunging fold axes (Berger & Jayasinghe, 1976). Fold axes of early isoclinal folds and late upright folds are parallel to L_2. The Wanni and Kadugannawa Complexes have been interpreted as fold nappes, which were emplaced on top of the Highland Complex with a top-to-the-NNW movement sense parallel to L_2 (Kriegsman, 1994). This main deformational event occurred at the peak of metamorphism. Partial breakdown of peak metamorphic assemblages to retrograde symplectites of various assemblages post-dates S_2.

Petrologic research has concentrated on metamorphosed basaltic–gabbroic to intermediate rocks (Sandiford *et al.*, 1988; Schumacher *et al.*, 1990; Faulhaber & Raith, 1991; Schumacher & Faulhaber, 1994), acid charnockites (Prame, 1991*a*) and metamorphosed pelitic rocks (Prame, 1991*b*; Hiroi *et al.*, 1994; Raase & Schenk, 1994). These investigations have established a pressure zonation across the Sri Lankan granulite terrane. Pressures and temperatures decrease roughly from 9–10 kbar and ~830°C in the east and southeast to 5–6 kbar and ~700°C in the northwest (Faulhaber & Raith, 1991; Schumacher & Faulhaber, 1994). The P–T path for pelitic rocks, based on the sequence kyanite (early, inclusions in garnet) followed by sillimanite (pervasive) followed by andalusite (rare, texturally late), is clockwise (Hiroi *et al.*, 1990; Raase & Schenk, 1994). By contrast, reaction textures involving pyroxenes, plagioclase, garnet and quartz in some metamorphosed igneous rocks (Schumacher *et al.*, 1990; Prame, 1991*a*) and high temperatures

(>900°C) from pyroxene exsolution (Schenk *et al.*, 1988) have been used by these workers as an indication of isobaric cooling, which apparently is not documented in the pelitic rocks and occurred before uplift.

The present study focuses on the petrology of Ca-poor, Mg-rich granulites from two localities in central Sri Lanka, which are found in the same general region as the pelitic rocks that have been studied by Raase & Schenk (1994) and the highest grade rocks reported by Schumacher & Faulhaber (1994). Reaction textures in these rocks have recorded the *P–T* segment close to peak temperature conditions, and provide a possible link between the information that has been obtained from metamorphosed pelitic and igneous rocks. This paper gives an account of reaction textures and gives evidence for sequential crossing of univariant boundaries for reactions in a model FeO–MgO–Al_2O_3–SiO_2 system. The reaction slopes suggest a *P–T* path with a roughly clockwise trajectory. The earlier, garnet-forming reactions probably formed during a heating phase that may or may not have been combined with a slight *P* increase. Both the orientations of the model reactions and the TWEEQU thermobarometry (Berman, 1991; Lieberman & Petrakakis, 1991) suggest that the reactions that produced the corona textures and the cordierite are the result of near-isothermal decompression.

OUTCROP AND SAMPLE DESCRIPTION

Sapphirine-bearing granulites were found in two localities in the central Highland Complex southeast of Kandy (Kriegsman, 1991*a*; see also Fig. 1). Osanai (1989) reported sapphirine- and kornerupine-bearing granulites from the same area. On the new road leading to Randenigala Dam and near the village of Hakurutale, sapphirine-bearing granulites form several lenses in a quartzitic matrix alternating with thin metapelitic layers (Fig. 2a). Metamorphosed basic gneisses are present 1 m below these lenses. The rocks are crumbly, but show few signs of weathering. This outcrop lies in the hinge zone of an upright NNW–SSE trending synform that refolds the main gneissic layering (S_2). The exposed lenses have formed by layer-parallel extension of either two parallel layers or larger lenses; the result was the formation of boudins with sizes ranging from 2 m × 5 m down to 5 cm × 5 cm. Separations between the boudins locally amounts to 1·5 m parallel to the L_2 stretching lineation. Inflow of quartzite into the necks of pinch-and-swell structures can be observed (Fig. 2b). Locally, monomineralic zones of garnet up to 5 cm wide and 40 cm long are present; these may be related to the break-up of the original layers.

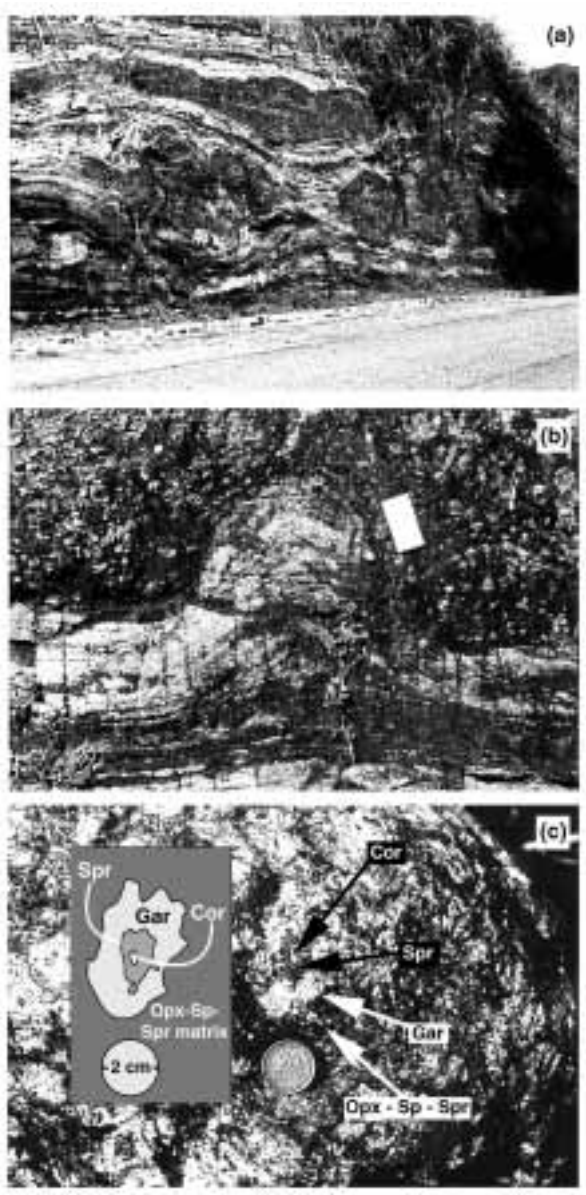

Fig. 2. Outcrop photographs. (a) Hakurutale sapphirine-bearing lenses in a road cut. (b) Pinch-and-swell of Hakurutale sapphirine-bearing lenses with inflow of quartzitic matrix (compass for scale). (c) The Munwatte boulder: corundum (Cor) and sapphirine (Spr) are separated from orthopyroxene (Opx), spinel (Sp) and sapphirine (Spr) in the matrix by garnet (Gar).

Samples from the Hakurutale lenses are dominated by prismatic orthopyroxene and sillimanite and porphyroblastic garnet. On the basis of modal proportions and the distribution of quartz and sapphirine, the relative silica content of the boudin decreases from the rim of the lenses to the core. Garnets in samples from the core commonly enclose sapphirine and rarely quartz; whereas those from the rim enclose quartz, but never sapphirine

Table 1: Mineralogy of thin sections

Zoned assemblages	Hakurutale			Munwatte	
	core[1]	intermediate[1]	rim[1]	+ patches[2]	– patches[2]
Orthopyroxene	× ×	× ×	× ×	× ×	× ×
Garnet	× ×	× ×	× ×	× ×	—
Sapphirine	× ×	×	—	× ×	× ×
Cordierite	× ×	× ×	× ×	× ×	×
Spinel	—	—	×	× ×	×
Sillimanite	× ×	× ×	× ×	×	—
Quartz	—	×	× ×	—	—
Corundum	—	—	—	× ×	—
Gedrite	—	—	—	×	—
Plagioclase	×	×	× ×	×	×

×, accessory; × ×, abundant; —, not present. Biotite, rutile, zircon and apatite also present.
[1]Core, intermediate and rim refer to position of samples in the Hakurutale lenses.
[2]Patches refers to composite textures with garnet, sapphirine, spinel, corundum, orthopyroxene in Munwatte samples.

(Table 1). Quartz is only part of the matrix assemblage in samples from the rim. Secondary corona structures are most common in quartz-rich samples. Most coronas and symplectites (Fig. 3) are the products of garnet + quartz and/or sillimanite breakdown. Symplectites of orthopyroxene + cordierite are the most common, and coronas of sapphirine + cordierite are common where quartz is absent. Orthopyroxene and sillimanite locally form symplectitic intergrowths rimming garnet. Plagioclase appears only in quartz-bearing samples from the rims of the lenses and commonly forms rounded inclusions in orthopyroxene–cordierite symplectites. Rutile, spinel, apatite, and zircon are accessory phases (Table 1).

The second locality is near the village of Munwatte (Fig. 1), where a loose boulder (Fig. 2c) containing large (up to 3 cm) sapphirine crystals was found on top of a river outcrop near milepost 29. The river has a very restricted catchment area, in which the source rock for this boulder must be located. In addition, no major tectonic discontinuities have been observed in this area. This block was probably a small tectonic lens, resembling the Hakurutale boudins. The river outcrop is composed of interlayered quartzites, metapelitic gneiss, charnockites and intermediate basic granulites. Garnet- and hornblende-rich lenses exist in these metamorphosed basic rocks and marbles crop out nearby. These rocks display L–S tectonic fabrics (L_2–S_2) similar to those at the Hakurutale locality (Kriegsman, 1991*b*). This outcrop is situated in a steep shear zone bordering the western limb of a doubly plunging synform (Fig. 1).

The most conspicuous texture in the Munwatte sample is the homogeneous distribution of large (up to 4 cm × 6 cm) patches that contain abundant corundum, sapphirine and garnet, in a matrix dominated by phlogopite and orthopyroxene (Figs 2c and 3a). Spinel, gedrite and corundum form inclusions in sapphirine. Cordierite commonly occurs in symplectites with orthopyroxene rimming garnet. Sillimanite is rare and is generally separated from either orthopyroxene or garnet by a rim of cordierite–sapphirine symplectite. Accessory minerals are rutile, zircon and apatite (Table 1).

PETROGRAPHY

Inclusion textures

Garnets in the samples from the Hakurutale locality contain isolated inclusions of orthopyroxene, sillimanite, sapphirine, quartz and biotite, and multiple inclusions of orthopyroxene + sapphirine (Table 2). Quartz is never in contact with sapphirine and, within garnet, orthopyroxene is never in contact with sillimanite.

Garnets in the samples from Munwatte locality contain isolated inclusions of sapphirine, orthopyroxene, rutile, apatite, biotite and, rarely, plagioclase (Table 2). Garnet–corundum contacts are very uncommon. Orthopyroxene inclusions in garnet are only rarely in contact with sapphirine. Generally, orthopyroxene is enclosed at garnet rims, whereas sapphirine is restricted to garnet cores (Fig. 3a).

Sapphirine grains from Munwatte that are enclosed in garnet generally exhibit multiple inclusions of gedrite + spinel, gedrite + corundum and spinel + corundum (Fig. 3a, Table 2). These sapphirines also enclose rutile, apatite and biotite. Corundum and apatite form

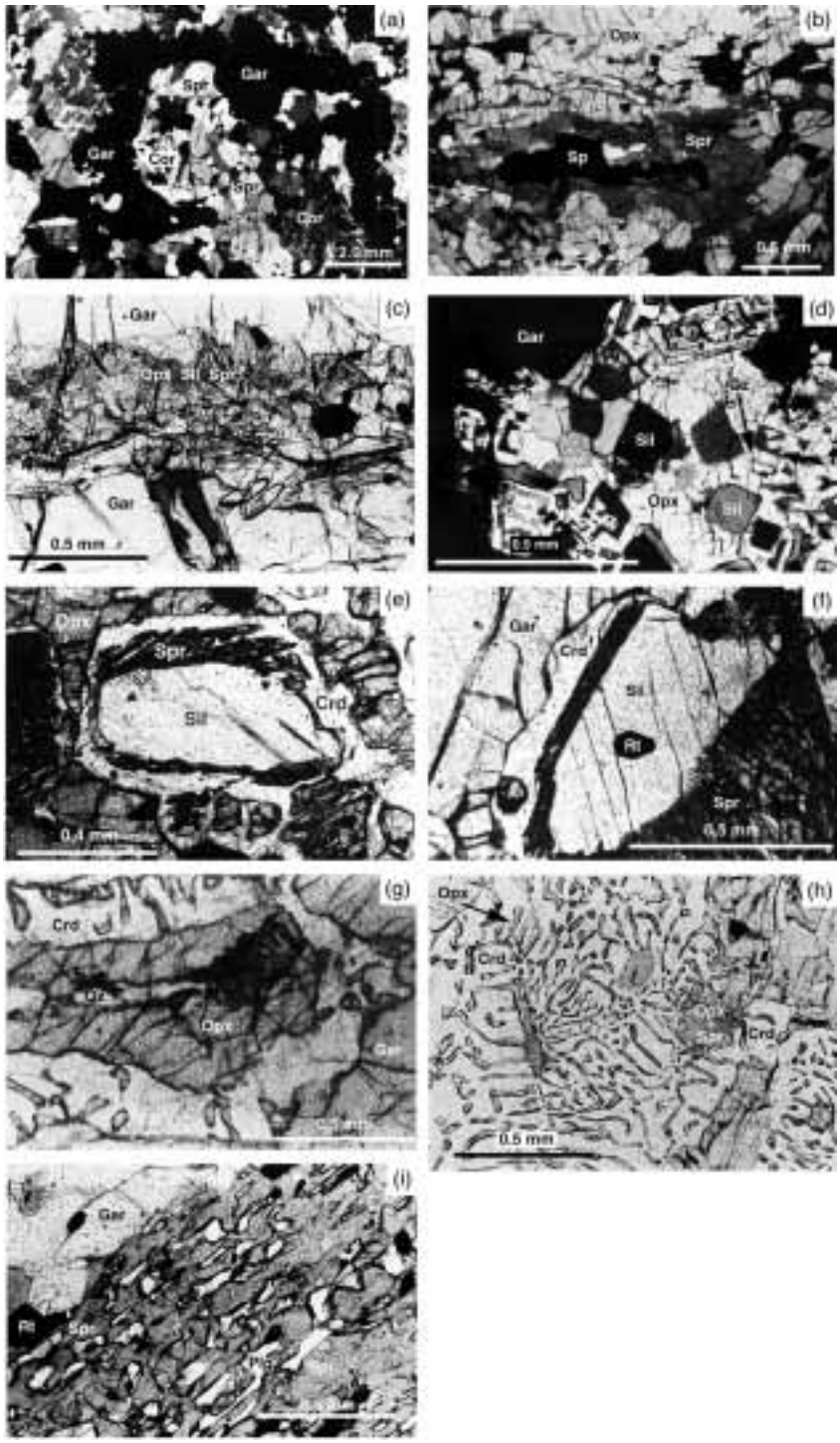

Fig. 3. Reaction textures in the Hakurutale (Hak) and Munwatte (Mun) sapphirine-bearing granulites. Crd, cordierite; Spr, sapphirine; Opx, orthopyroxene; Sp, spinel; Gar, garnet; Plg, plagioclase; Sil, sillimanite; Qz, quartz; Cor, corundum; Rt, rutile. (a) Spr corona around Cor that separates Gar and Cor; Opx is present in the outer rim of Gar (Mun); (b) rim of Spr between Opx and Sp (Mun); (c) Gar replaced by Opx + Sil + Spr in a fracture (Mun); (d) Opx–Sil symplectite replacing Gar + Qz (Hak); (e) Spr–Crd symplectite separating Opx and Sil (Hak); (f) Spr–Crd symplectite separating Gar and Sil (Hak); (g) sequential assemblages of Qz–Opx–(Crd + Opx)–Gar, suggesting the reaction Gar + Qz = Opx + Crd (Hak); (h) Opx–Spr symplectite + Crd replacing Gar (Mun); (i) Spr–Plg symplectite replacing Gar (Mun).

Table 2: Mineral inclusions in sapphirine and garnet

Zoned assemblages	Hakurutale			Munwatte	
	core[1]	intermediate[1]	rim[1]	+ patches[2]	– patches[2]
Ged in Spr	—	—	—	×	—
Cor in Spr	—	—	—	×	—
Sp in Spr	—	—	—	×	×
Rt in Spr	—	—	—	×	—
Apt in Spr	—	—	—	×	—
Sil in Gar	×	×	×	—	no Gar
Opx in Gar	×	×	×	×	no Gar
Qz in Gar	—	×	×	—	no Gar
Spr in Gar	×	×	—	×	no Gar
Rt in Gar	×	×	×	×	no Gar

Crd, cordierite; Spr, sapphirine; Opx, orthopyroxene; Sp, spinel; Gar, garnet; Plg, plagioclase; Sil, sillimanite; Qz, quartz; Cor, corundum; Rt, rutile; Apt, apatite. ×, present; —, not present; 'no Gar', no garnet is present.
[1]Core, intermediate and rim refer to position of samples in the Hakurutale lenses.
[2]Patches refers to composite textures with garnet, sapphirine, spinel, corundum, orthopyroxene in Munwatte samples.

the inclusions in sapphirine cores, whereas gedrite, biotite, spinel and rutile are more abundant away from the cores.

Corona and symplectite textures common to both localities

Orthopyroxene symplectite and corona structures

Orthopyroxene–sillimanite symplectites are common in the quartz-bearing samples of Hakurutale (Table 3). These occur as coarse intergrowths with individual crystals up to 3·0 mm × 0·8 mm that rim garnet and quartz, blocky intergrowths with sillimanite prisms that have end-sections up to 150 μm across (Fig. 3d), ribbon symplectites with individual widths of 10–50 μm, and plume-like intergrowths with 5–30 μm thick blades. These symplectites generally rim garnet and locally separate garnet and quartz, and are commonly separated from quartz by an orthopyroxene corona. Locally, plagioclase is present in these symplectites. Orthopyroxene–sillimanite intergrowths are rare at Munwatte, where they are associated with biotite.

Coronas and symplectites with orthopyroxene and cordierite are present at both localities, but appear to have formed by various mechanisms. Coronas with orthopyroxene and cordierite that separate garnet and quartz (Fig. 3g) occur only in the quartz-bearing Hakurutale samples (Table 3). Here, orthopyroxene occurs invariably adjacent to quartz, cordierite next to garnet. The thickness of these rims can be up to 0·3 mm. Orthopyroxene–cordierite symplectites generally consist of about 60–80 vol. % cordierite and 40–20 vol. % orthopyroxene blades with widths of 20–120 μm. The same type of symplectite also occurs between garnet and biotite grains both in the Hakurutale and in the Munwatte samples.

Sapphirine is commonly present in very fine-grained orthopyroxene–sapphirine symplectites within the coarser orthopyroxene–cordierite symplectites, suggesting sapphirine formed at a late stage in these reaction rims.

Orthopyroxene–plagioclase symplectites with or without cordierite locally separate garnet and biotite in the Munwatte samples, and garnet and quartz in the Hakurutale samples. The amount of orthopyroxene is similar to that in orthopyroxene–cordierite symplectites. The amount of plagioclase present is correlated with the amount of grossular component in the garnet that is being replaced. More rarely, some of the Hakurutale samples display orthopyroxene–plagioclase rims and symplectites, which separate garnet from quartz.

Lamellar orthopyroxene–sapphirine symplectites (Fig. 3c) are found at the rims of both garnet and prismatic orthopyroxene in all samples. Their lamellae are <30 μm wide. These symplectites have also been observed at the contact of garnet and orthopyroxene inclusions, indicating a retrograde re-equilibration of Al in orthopyroxene with the contiguous garnet. The symplectites also occur in orthopyroxene–cordierite symplectites replacing garnet in samples lacking quartz. Coarse-grained orthopyroxene–sapphirine intergrowths are present in the matrix of the Munwatte samples.

Table 3: Zoned assemblages in thin sections

Zoned assemblages[1]	Hakurutale			Munwatte	
	core[2]	intermediate[2]	rim[2]	+ patches[3]	patches[3]
Cor > Spr > Gar	—	—	—	×	—
Cor > Spr + Plg > Gar	—	—	—	×	—
Sp > Spr > Gar	—	—	—	×	—
Sp > Spr > Opx	—	—	—	—	×
Gar > Opx + Sil > Qz	—	×	×	o	—
Gar > Opx + Sil + Spr	×	×	—	×	—
Gar > Opx + Crd > Qz	—	×	×	o	—
Gar > Opx + Crd + Spr	×	×	—	×	—
Gar > Spr + Crd > Sil	×	×	×	×	—
Opx > Spr + Crd > Sil	×	×	×	×	—
Gar > Crd > Sil	—	—	×	—	—
Gar > Crd > Qz	—	—	×	—	—
Sil > Crd > Qz	—	—	×	—	—
Opx > Crd > Sil	—	—	×	—	—
Opx > Crd > Qz	—	—	×	—	—
Gar > Crd + Sp > Sil	—	—	×	—	—
Gar > Opx + Plg > Qz	—	—	×	—	—
Bio > Crd > Gar	—	—	—	×	—
Bio > Crd > Plg	—	—	—	×	—

Crd, cordierite; Spr, sapphirine; Opx, orthopyroxene; Sp, spinel; Gar, garnet; Bio, biotite; Plg, plagioclase; Sil, sillimanite; Qz, quartz; Cor, corundum. ×, present; —, not present; o, present, but biotite replaces quartz in the zoned sequence.
[1]Gar > Opx + Sil > Qz indicates Gar and Qz are separated by an Opx–Sil symplectite.
[2]Core, intermediate and rim refer to position of samples in the Hakurutale lenses.
[3]Patches refers to composite textures with garnet, sapphirine, spinel, corundum, orthopyroxene in Munwatte samples.

Sapphirine–cordierite symplectites and plagioclase overgrowths

Sapphirine–cordierite symplectites are especially abundant in parts of the Hakurutale samples lacking matrix quartz. Sapphirine grains have widths of 15–100 μm and separate either sillimanite from orthopyroxene (Fig. 3e) or sillimanite from garnet (Fig. 3f). Where sapphirine is larger, it forms sheaves in cordierite. Sapphirine–cordierite symplectites are rarer in Munwatte, but they do occur.

In a few places plagioclase overgrowths formed at grain boundaries between orthopyroxene and matrix plagioclase. Plagioclase in these rims, which are ~20 mm wide, invariably has a higher anorthite component than the earlier matrix plagioclase.

Textures restricted to the Munwatte locality

Sapphirine commonly overgrows spinel in the orthopyroxene-bearing matrix (Fig. 3b) and separates garnet and corundum within the garnet patches (Fig. 3a). In both cases, sapphirine is coarse grained. The corona structures within the garnet are more complex; here, the sapphirine may enclose gedrite, corundum or spinel. The outermost parts of these enclosing sapphirines are generally inclusion free. Away from the sapphirine, at the interface with the matrix, the garnet may enclose orthopyroxene.

Intergrowths of sapphirine and plagioclase (Fig. 3i) are inclusions within garnet in only two thin sections. The ratio of plagioclase to sapphirine is 1:2 to 1:3. Other sapphirine inclusions in the same garnets contain corundum.

In addition to the modes of occurrence outlined above, cordierite occurs at biotite–garnet or biotite–plagioclase grain boundaries. This has been observed in only a limited number of cases in the Munwatte samples.

MINERALOGY

Analytical procedure

Minerals were analysed with a JEOL JXA-8600 Superprobe at 15 kV and 10 nA at the University of

Table 4: Representative microprobe analyses of garnet

	Gar[1]	Gar[2]	Gar(6)	Gar(5)	Gar(g)	Gar(11)	Gar(14)	Gar(13)	Gar(3&1)	Gar(20)
Point:	592	1424	1326	262	1162	336	150	241	685	123
SiO_2	41·12	39·78	40·78	40·80	40·80	40·52	40·50	39·69	41·57	40·58
TiO_2	0·00			0·05		0·00	0·03	0·02	0·03	0·00
Al_2O_3	23·32	22·60	22·98	23·39	23·28	22·96	22·90	22·45	23·15	23·09
FeO	15·76	22·93	21·66	17·74	16·38	18·64	17·60	22·03	15·61	20·08
MnO	0·10	0·31	0·23	0·08	0·18	0·00	0·21	0·34	0·00	0·21
MgO	18·95	13·15	14·82	17·26	17·59	15·70	16·83	14·26	18·39	13·80
CaO	1·20	1·32	0·85	1·11	1·46	1·27	0·99	1·15	1·29	3·05
Total	100·45	100·09	101·32	100·43	99·69	99·21	99·89	99·94	100·04	100·81
Structural formulae: 8 cations per 12 oxygens or 12 oxygens										
Si	2·953	2·978	2·988	2·961	2·971	3·002	3·001	2·957	3·003	2·989
Al	1·974	1·994	1·985	2·001	1·998	2·005	1·997	1·972	1·971	2·005
Ti	0·000	0·000	0·000	0·003	0·000	0·000	0·002	0·001	0·002	0·000
Fe^{3+}	0·121	0·051	0·039	0·072	0·061	0·000	0·000	0·112	0·019	0·017
Mg	2·029	1·467	1·619	1·867	1·909	1·734	1·834	1·584	1·981	1·515
Fe^{2+}	0·826	1·385	1·288	1·005	0·936	1·155	1·076	1·261	0·924	1·220
Mn	0·006	0·020	0·014	0·005	0·011	0·000	0·013	0·021	0·000	0·013
Ca	0·092	0·106	0·067	0·086	0·114	0·101	0·078	0·092	0·100	0·241
Cations	8·000	8·000	8·000	8·000	8·000	7·996	7·999	8·000	8·000	8·000
X_{Mg}	0·711	0·514	0·557	0·650	0·671	0·600	0·630	0·557	0·682	0·554

Gar numbers in parentheses refer to assemblages mentioned in the text (see also Table 8). X_{Mg} = Mg/(Mg + Fe^{2+}).
[1]Highest X_{Mg}.
[2]Lowest X_{Mg}.

Utrecht. Both mineral and synthetic compounds were used as standards. Raw count data were corrected with a Tracor Northern PROZA correction program. Representative analyses of the relevant mineral phases are presented in Tables 4–6. Ferric iron estimations for the structural formulae of spinels, sapphirines, garnets, pyroxenes and gedrites were carried out using stoichiometric constraints (Robinson *et al.*, 1982; Droop, 1987; Schumacher, 1991); no ferric estimations were carried out for biotite or cordierite.

Garnet

Garnet commonly forms large porphyroblasts (up to 3 cm). It is pink to dark red in hand specimen and pale pink in thin section. Garnet in the Hakurutale samples can enclose orthopyroxene, sillimanite, quartz or sapphirine; Munwatte garnet encloses sapphirine aggregates and orthopyroxene (see corona descriptions). Rutile, apatite and biotite are also common inclusions. Grossular and spessartine components are low, with maximum X_{Ca} and X_{Mn} of 0·09 and 0·007, respectively, in both localities (Table 4). The X_{Mg} is 0·53–0·68 at Hakurutale and 0·60–0·72 at Munwatte (Fig. 4); these are among the highest Mg contents reported for granulite-facies garnets and are slightly higher than values reported by Harley & Fitzsimons (1991) from the Rauer Group in east Antarctica. Garnet X_{Mg} shows considerable variation per reaction texture (Table 7) and is highest in assemblages with corundum and lowest in quartz-bearing assemblages, which explains the difference in X_{Mg} range between the two localities.

Orthopyroxene

Orthopyroxene is present as prismatic grains (up to 2 cm in Hakurutale, 5 mm in Munwatte) in the matrix, as inclusions in garnet and in symplectites. It has a bronze colour in hand specimen and is pleochroic in thin section: pink parallel to the x vibration direction and pale green parallel to the y and z vibration directions. Its $2V_x$ is 80–90°. Matrix orthopyroxenes in the Hakurutale samples show strong preferred orientation and evidence for rotation recrystallization. Secondary orthopyroxene occurs in intergrowths with sapphirine, cordierite or sillimanite. The range of X_{Mg} is 0·76–0·87 at Hakurutale and 0·79–0·87 at Munwatte (Table 5 and Fig. 4a). The

Table 5: Representative microprobe analyses of orthopyroxene

Point:	Opx(13)[1] 1343	Opx(5)[2] 264	Opx(7) 1333	Opx(11) 1203	Opx(1) 673
SiO_2	53·40	50·00	50·68	52·26	51·86
TiO_2	0·00	0·15	0·00	0·00	0·10
Al_2O_3	2·78	10·30	7·20	5·74	7·84
FeO	15·73	10·82	15·41	14·02	10·95
MnO	0·00	0·08	0·00	0·00	0·00
MgO	28·09	28·42	26·68	27·24	29·55
CaO	0·22	0·00	0·08	0·14	0·08
Total	100·37	99·77	100·28	100·06	100·38
Structural formulae: 4 cations per 6 oxygens					
Si	1·908	1·758	1·811	1·875	1·812
Al(4)	0·092	0·242	0·189	0·125	0·188
Al(6)	0·025	0·185	0·115	0·117	0·135
Ti	0·000	0·004	0·000	0·000	0·003
Fe^{3+}	0·067	0·048	0·074	0·008	0·048
Mg	1·496	1·490	1·422	1·457	1·539
Fe^{2+}	0·403	0·270	0·387	0·413	0·272
Mn	0·000	0·002	0·000	0·000	0·000
Ca	0·008	0·000	0·003	0·005	0·003
Sum	4·000	4·000	4·000	4·000	4·000
X_{Mg}	0·788	0·847	0··786	0·779	0·850

Opx numbers in parentheses refer to assemblages mentioned in the text (see also Table 8). $X_{Mg} = Mg/(Mg + Fe^{2+})$.
[1]Lowest Al content.
[2]Highest Al content.

X_{Mg} shows little variation between reaction textures, but is highest in assemblages lacking quartz (assemblages 1, 5 and 16 in Table 7). Not surprisingly, Ca content is very low (<0·010 per six oxygens). The octahedral Al may be as high as 0·184 in orthopyroxenes from both outcrops, with a maximum of 10·3 wt % Al_2O_3 (Table 5). The average octahedral Al is lower in the symplectitic orthopyroxene than in cores of prismatic grains. Highest Al values were measured in texturally early assemblages 1 and 5 (Table 7). Orthopyroxenes associated with plagioclase have lowest Al values. Locally, the orthopyroxenes in coronas and symplectites are strongly zoned with respect to aluminum (Fig. 4b and c), with lowest Al values adjacent to quartz and sillimanite, and highest values next to cordierite and garnet. The X_{Mg} does not show this variation, which suggests it is not a later retrograde phenomenon, but may reflect a diffusion gradient.

Cordierite

Cordierite is commonly associated with orthopyroxene in coronas or symplectites separating garnet and quartz. Cordierite is also present as large inclusion-free grains up to 1 cm across that apparently replace garnet in the Hakurutale samples. In addition, it occurs in symplectites with sapphirine that separate sillimanite from either orthopyroxene or garnet. This type of occurrence is more common in the Hakurutale samples. Where visible in hand specimen, cordierite has a transparent deep blue colour. The $2V_z$ is 80° and axial dispersion is $r<v$. Cordierite exhibits characteristic, tapering polysynthetic twin lamellae, which are less well defined than those in plagioclase and reflect the pseudo-hexagonal symmetry of cordierite. Yellow pleochroic haloes surround zircon or monazite inclusions. Cordierite is highly magnesian, irrespective of the assemblage (Table 7 and Fig. 4a), with X_{Mg} 0·89–0·94 in both localities (Table 6). The Na_2O contents are <0·1 wt %. No attempt was made to test directly for volatile components in cordierite; however, analytical sums range between about 98 and 100%, which suggests that volatile constituents could be present in the channels of some of the cordierite (e.g. Selkregg & Bloss, 1980). The birefringence is ~0·009 in all samples, which indicates that, if appreciable amounts of channel fluid are actually present, this fluid would be H_2O dominated, rather than rich in CO_2, which would increase the birefringence to ~0·012–0·014.

Sapphirine

Sapphirine is abundant in the Munwatte samples, where it forms aggregates up to 3 cm across, with individual grains up to 5 mm across, both in the matrix and enclosed by garnet porphyroblasts. Matrix sapphirine is subhedral, and sapphirine in garnet anhedral. It is dark greyish blue in hand specimen and shows blue pleochroic colours in thin section, varying from pale, azure blue parallel to the z vibration direction to greenish blue and azure blue parallel to the y vibration direction. Its $2V_x$ is 50–60° with strong axial dispersion ($r<v$). Sapphirine enclosed by garnet contains large corundum grains and small amounts of spinel, gedrite, biotite, rutile and apatite. Matrix sapphirine encloses only spinel, biotite, rutile and apatite, and is commonly associated with orthopyroxene and biotite. In the Hakurutale samples sapphirine occurs only as inclusion-free grains up to 1 mm across that are enclosed in garnet.

In samples from both outcrops, secondary sapphirine is found in lamellar intergrowths with orthopyroxene at orthopyroxene–garnet grain boundaries, symplectites with cordierite separating sillimanite from either garnet or orthopyroxene (extensively developed in the Hakurutale samples), sapphirine–orthopyroxene–sillimanite aggregates rimming garnet, and rare symplectites with plagioclase separating garnet and corundum (Munwatte).

Table 6: Representative microprobe analyses of minerals

Analysis:	Crd 32	Crd 180	Spr[1] 662	Spr[2] 1104	Sp 664	Ged 1116	Ged 83
wt %							
SiO_2	50·87	49·76	12·00	13·61	0·00	44·52	42·08
TiO_2	—	0·00	0·03	0·07	0·00	0·67	0·97
Al_2O_3	34·50	33·58	65·13	62·13	64·43	17·50	19·95
Cr_2O_3	—	—	0·16	0·19	0·32	0·13	0·00
FeO	1·81	2·01	5·02	5·58	15·27	9·48	9·39
MnO	0·05	0·00	0·00	0·00	0·00	0·09	0·12
MgO	12·49	12·55	16·95	18·44	16·90	22·27	21·29
ZnO	—	—	—	0·00	3·10	0·00	0·00
CaO	0·07	0·00	0·00	0·00	—	0·52	0·49
Na_2O	0·08	0·15	0·01	0·03	—	2·16	2·64
K_2O	0·00	0·00	0·00	0·00	—	0·00	0·08
F	—	—	0·02	—	—	0·40	0·47
Cl	—	—	0·02	—	—	0·00	0·00
H_2O[3]						1·96	1·91
Total	99·87	98·03	99·34	100·05	100·02	99·17	98·72
Structural formulae							
Si	4·999	4·993	1·419	1·598	0·000	6·206	5·912
Al(4)	1·001	1·007	4·581	4·402	0·000	1·794	2·088
Al(6)	2·995	2·964	4·496	4·195	1·956	1·081	1·215
Ti	0·000	0·002	0·003	0·006	0·000	0·070	0·103
Cr	0·000	0·000	0·015	0·018	0·007	0·014	0·000
Fe^{3+}	0·000	0·000	0·067	0·184	0·037	0·000	0·000
Mg	1·830	1·877	2·988	3·227	0·649	4·628	4·468
Fe^{2+}	0·149	0·169	0·430	0·364	0·292	1·062	1·106
Mn	0·004	0·000	0·000	0·000	0·000	0·011	0·014
Zn	—	—	0·000	0·000	0·059	0·000	0·000
Ca	0·007	0·000	0·000	0·000	0·000	0·078	0·074
Na	0·015	0·025	0·002	0·007	—	0·584	0·719
K	—	—	—	—	—	—	0·014
F	—	—	0·007	—	—	0·176	0·209
Cl	—	—	0·004	—	—	—	—
X_{Mg}	0·925	0·917	0·874	0·899	0·694	0·813	0·802

Structural formulae are calculated using the following stoichiometric assumptions: cordierite (Crd)—18 oxygen (no ferric iron estimation); sapphirine (Spr)—14 cations, 20 oxygen; spinel (Sp)—3 cations, 4 oxygen; gedrite (Ged)—23 oxygen, all ferrous formulae. $X_{Mg} = Mg/(Mg + Fe^{2+})$. —, not analysed or detected.
[1]Highest Al content.
[2]Lowest Al content.
[3]Estimated.

Sapphirine is very magnesian: X_{Mg} is 0·81–0·95 in both localities (Table 6 and Fig. 4a). The Al + Fe^{3+} content varies from 8·41 and 9·29, with an average of ~8·8 in all assemblages (Tables 6 and 7). In sapphirine–spinel pairs (only Munwatte), $Fe^{3+}/(Fe^{3+} + Fe^{2+})$ is always higher in sapphirine, similar to the occurrences reported by Caporuscio & Morse (1978) and Lal *et al.* (1984).

Spinel

In the Munwatte samples, spinel occurs as grains (up to 1 mm) enclosed by sapphirine that, locally, are in contact with corundum. At Hakurutale it occurs as tiny grains (maximum 0·07 mm across) in orthopyroxene–cordierite symplectites in quartz-bearing samples. It is green in all samples. The X_{Mg} ranges from 0·66 to 0·73 (Table 6 and Fig. 4a). The average ZnO content is only 2·43 wt %, corresponding to 5·3% substitution of Zn for (Mg, Fe^{2+}). The $Fe^{3+}/(Fe^{3+} + Fe^{2+})$ is consistently lower than in contiguous sapphirine (above). Magnetite exsolution lamellae are not present.

Gedrite

Gedrite is present only as small (up to 100 μm), isolated inclusions in sapphirine. It shows pale brown pleochroic

Table 7: Mineral chemistry for reaction assemblages that involve cordierite (Crd), sapphirine (Spr), orthopyroxene (Opx), spinel (Sp), garnet (Gar), sillimanite (Sil), quartz (Qz), corundum (Cor), gedrite (Ged) and plagioclase (Plg)

Reaction assemblage		X_{Mg}^{Gar}		X_{Mg}^{Opx}		X_{Al}^{Opx}		X_{Mg}^{Spr}		Al pfu		X_{Mg}^{Crd}	X_{Mg}^{Sp}	X_{Ca}^{Plg}
	No.	Range	Av. (*n*)[1]	Range	Av. (*n*)[1]	Range	Av. (*n*)[1]	Range	Av. (*n*)[1]	Range	Av. (*n*)[1]	range	range	range
Opx + Cor = Gar	1	0·64–0·71	0·67 (46)	0·81–0·86	0·83 (29)	0·15–0·19	0·17 (29)					—	—	—
Sp + Gar + Cor = Spr	3	0·65–0·71	0·68 (29)	—	—	—	—	0·87–0·91	0·89 (42)	8·6–9·1	8·7 (42)	—	0·68–0·70	—
Gar = Spr + Opx + Sil	5[2]	0·59–0·68	0·65 (12)	0·81–0·87	0·83 (26)	0·12–0·22	0·16 (26)	0·88–0·93	0·89 (4)	8·7–8·8	8·8 (4)	—	—	0·48–0·49
Gar + Qz = Opx + Sil	6[2]	0·52–0·63	0·59 (26)	0·76–0·84	0·80 (30)	0·09–0·15	0·13 (30)	—				—	—	0·23–0·37
Opx + Sil + Qz = Crd	7[2]	—	—	0·75–0·79	0·76 (5)	0·10–0·15	0·12 (5)	—				0·92–0·93	—	0·33
Gar + Sil + Qz = Crd	9[2]	0·64–0·68	0·66 (3)	—	—	—	—	—	—	—	—	0·90–0·99		0·41–0·50
Opx + Sil = Crd + Spr	10[2]	—	—	0·76–0·83	0·80 (26)	0·12–0·17	0·14 (26)	0·83–0·92	0·88 (20)	8·6–8·9	8·8 (20)	0·92–10·00	—	—
Gar + Qz = Opx + Crd	11[2]	0·57–0·67	0·61 (19)	0·74–0·83	0·79 (59)	0·07–0·18	0·13 (59)	—	—	—	—	0·91–10·00	—	0·24–0·42
Gar + Sil = Crd + Spr	13[2]	0·53–0·64	0·58 (5)	—	—	—	—	0·81–0·90	0·86 (17)	8·6–8·8	8·7 (17)	0·90–0·99	—	—
Gar = Crd + Spr + Opx	14[2]	0·52–0·64	0·60 (22)	0·78–0·85	0·81 (41)	0·11–0·17	0·13 (41)	0·85–0·92	0·89 (29)	8·4–9·0	8·8 (29)	0·92–0·99	—	0·80–0·85
Gar + Sil = Crd + Sp	16[2]	—	—	0·83	0·83 (1)	0·13	0·13 (1)	—				0·93	0·70–0·72	—
Gar + Cor = Spr + Plg	1.7	0·67–0·68	0·68 (4)	—	—	—	—	0·89	0·89 (1)	8·7	8·7 (1)	—	—	0·48–0·53
Gar + Qz = Opx + Plg	20[2]	0·52–0·65	0·57 (16)	0·76–0·80	0·78 (10)	0·08–0·16	0·12 (10)	—	—	—	—	—	—	0·22–0·39

Numbers are the same as in the text. Compositions are within the same range for similar assemblages in samples from the Hakurutale and Munwatte localities. No data available for assemblages with Opx + Sp + Spr ± Cor. X_{Mg} = Mg/(Mg + Fe^{2+}); X_{Al} = Al/2; X_{Ca} = Ca/(Ca + Na).
[1]Av. (*n*), average value of *n* measurements.
[2]Symplectitic textures; assemblages 5 and 6 show both a prismatic stage (Gar growth) and a symplectitic stage (Gar breakdown).

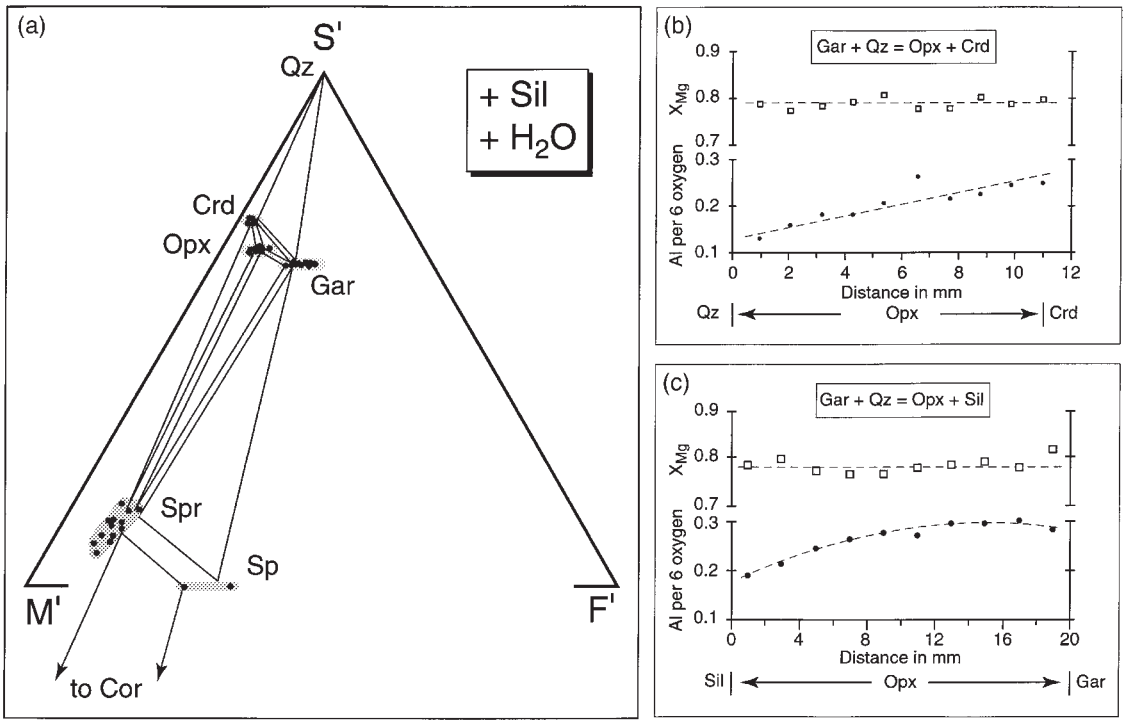

Fig. 4. (a) Representative compositions of cordierite (Crd), sapphirine (Spr), gedrite, orthopyroxene (Opx), spinel (Sp) and garnet (Gar) on a projection from sillimanite to the SiO_2–$MgAl_2O_4$–$FeAl_2O_4$ plane of an FeO–MgO–Al_2O_3–SiO_2 tetrahedron. It should be noted that not all phases actually coexist with sillimanite. (b, c) Profiles of Al vs distance through orthopyroxenes in assemblages Gar + Qz = Crd + Opx (b) and Gar + Qz = Opx + Sil (c). (See text for discussion.)

colours. The X_{Mg} is 0·83–0·91 (Table 6), which is comparable with sapphirine. It has a high average Na content of 0·648 (per 23 oxygen formula) and contains up to 0·1 Ca per 23 oxygen formula. The analyses indicate that F anions replace as much as 20% of the OH.

Plagioclase

Plagioclase is found in samples from both outcrops, but is only locally abundant. In those apparently more Ca-rich parts of the samples, it occurs as inclusions in garnet, intergrowths with sapphirine (Munwatte) in garnet interiors, symplectites with orthopyroxene ± cordierite replacing garnet, and plagioclase lenses rimming garnet. The X_{An} varies from 0·22 to 0·85 and is highest in assemblages with cordierite. Ca-poor plagioclase is locally separated from orthopyroxene by a thin rim of plagioclase with a higher anorthite content. This suggests a late-stage re-equilibration among garnet, orthopyroxene and plagioclase.

Biotite

Biotite is present as small inclusions in sapphirine, orthopyroxene and garnet, and as a major matrix mineral, notably in the Munwatte samples. All examples show normal, pale yellow to orange–brown pleochroism. The X_{Mg} is 0·85–0·89 in Hakurutale and 0·85–0·91 in Munwatte. The interlayer site is predominantly K, and K + Na is generally >0·950. The Ti content ranges from about 0·11 to 0·23 and the octahedral Al ranges from about 0·60 to 0·17 per 12 O, OH and F. Fluorine was detected in nearly every point analysis of biotite. The F contents are as high as 0·5 on the basis of 12 O, OH and F, but generally range between 0·15 and 0·30.

Quartz, sillimanite, corundum

Quartz is present in only the Hakurutale samples, notably in samples from the rim of the Hakurutale lenses. It commonly forms rounded inclusions (up to 1 mm across) in garnet. In the most silica-rich samples it occurs in the matrix, locally as ribbons (up to 10 cm × 1 cm). Matrix quartz is invariably separated from garnet either by orthopyroxene–cordierite coronas and symplectites or by orthopyroxene–sillimanite symplectites.

Sillimanite is a major phases in the Hakurutale samples, where prisms reach 2 cm in length. Texturally early grains show a well-developed grain shape and crystallographic preferred orientation parallel to the regional L_2 and

are commonly enclosed by garnet. Sillimanite does not enclose other phases. Its $2V_z$ is about 30°, it has strong axial dispersion ($r > v$) and shows the characteristic (010) cleavage in end sections. Secondary sillimanite occurs in symplectites with orthopyroxene replacing garnet and quartz. Sillimanite is rarer in the Munwatte samples, where it occurs as elongate prisms up to 3 mm in length in the matrix. It is associated with orthopyroxene, but is never enclosed by garnet. Sillimanite for both localities shows <1% substitution of Fe^{3+} or Cr for Al.

Corundum is present only in Munwatte. It occurs exclusively as armoured relicts in sapphirine and is locally in contact with spinel. Original grain size, deduced from optically continuous grains, was up to 1·0 cm × 0·5 cm. In only one place in one thin section has corundum been observed in contact with garnet. Corundum shows well-developed twins and, locally, much thinner deformation lamellae, and analyses indicate very little replacement of Al by Cr and Fe^{3+} ($\leq$0·7%).

Accessory minerals

The most abundant accessory mineral is rutile, which is present in every thin section and can be up to 2 mm in size. It is included in garnet, orthopyroxene, sapphirine and matrix biotite. The largest rutiles occur as inclusions in sapphirine and have <1% substitution of Cr or Fe^{3+} for Ti. Apatite is present as large (up to 0·5 mm) inclusions in garnet and sapphirine in the Munwatte samples. It further is present at locations where texturally late symplectites involving cordierite formed. Zircon is small and not abundant, and it causes conspicuous pleochroic haloes in cordierite and biotite.

Comparison of Hakurutale and Munwatte samples

The differences in mineralogy (corundum in Munwatte, quartz in Hakurutale) and modal distribution (sillimanite rare in Munwatte, abundant in Hakurutale) reflect different bulk-rock Al–Si ratios. The mineral chemistry of all constituent phases, however, is nearly identical in both localities and is characterized by high X_{Mg} ratios for all Fe–Mg phases. The order of decreasing X_{Mg} is Crd > Spr > Ged $\approx$ Bio > Opx > Sp > Gar, similar to that in other magnesian granulites (Hensen, 1987). Rutile is the most common accessory phase in all samples, and ilmenite, haematite and magnetite are absent.

TREATMENT OF CHEMICAL COMPONENTS

Graphical representations of the phase relations can be indispensable to evaluating properly complex sets of mineral assemblages and choosing appropriate petrogenetic grids to trace the evolution in P–T space. Samples from both localities are fully described by the system SiO_2–TiO_2–Al_2O_3–Cr_2O_3–Fe_2O_3–FeO–MnO–MgO–ZnO–CaO–Na_2O–K_2O–P_2O_5–H_2O–F. The components SiO_2–Al_2O_3–MgO–FeO are the principal constituents of spinel, corundum, Al-silicate and all the Mg-bearing silicate phases that are involved in the reactions. With one exception, the remaining components can be treated as trace, accessory or determining inert components (Korzhinskii, 1959), which do not influence the phase relations (net-transfer reactions) that explain the reaction textures.

In local assemblages where garnet is partially broken down and plagioclase is produced, CaO is an additional component involved in the net transfer reactions. The average grossular component of garnet is low (2·8%, Table 4). The CaO contents of the other phases are negligible (Tables 4–6), and, in most other cases, CaO is a trace component. Both plagioclase and gedrite contain Na_2O, but these phases do not participate in the same net transfer reactions. As a result, Na_2O may be treated as an accessory component. The K_2O is almost exclusively present in biotite and stabilizes that phase.

The ZnO, which is restricted to spinel, is treated as an accessory component. The maximum ZnO content in spinel is $\leq$3·4 wt % and can be explained by progressive Zn enrichment of relicts during spinel-consuming reactions (described below) or variation in the original ZnO content.

Ferric iron was not determined, but estimates that are based on mineral stoichiometry and the pleochroic colours of some of the minerals (e.g. biotite) suggest that Fe_2O_3 is only a minor constituent. Further, the absence of magnetite exsolution lamellae in spinel, free magnetite, or a free rhombohedral oxide phase suggest that these rocks were poor in Fe_2O_3 (Powell & Sandiford, 1988). Consequently, Fe_2O_3 is a trace component.

The MnO and Cr_2O_3 are trace components, because the garnets have <0·25 wt % MnO and all the remaining minerals have <0·1 wt % of both MnO and Cr_2O_3. The P_2O_5 behaves as an accessory component stabilizing apatite. The TiO_2 is an accessory component in rutile and a trace component in biotite and gedrite. Fluorine in gedrite (<0·50 wt %) is a trace component.

The components FeO–MgO–Al_2O_3–SiO_2 (FMAS) are the principal components of the most abundant phases and are adequate to describe the vast majority of net transfer and continuous Fe–Mg reactions. Most of the phase relations can be graphically portrayed in projections from quartz, sillimanite or corundum to selected planes in an FeO–MgO–Al_2O_3–SiO_2 tetrahedron (Robinson & Jaffe, 1969; Schumacher & Robinson, 1987). A few significant exceptions are discussed separately.

MODEL REACTION SEQUENCES

The descriptions that were given earlier show that the two localities share similarities in assemblage type and modes of occurrences and in mineral composition. Further, both localities have an early garnet-forming phase that was followed by partial destruction of the garnet via a varied set of reactions. In both localities, cordierite formed texturally later and, in part, as a breakdown product of garnet.

The most significant differences among the assemblages from the two localities seem to be caused by variation in SiO_2 activity (i.e. Si content) in bulk compositions. The Hakurutale locality is generally richer in SiO_2 and, as a consequence, most reactions involve quartz or sillimanite. The Munwatte locality was poorer in SiO_2, and corundum was stable in the earliest recognizable assemblages. At both localities, as the garnet-forming reactions commenced, various combinations of the phases quartz, sillimanite, corundum, sapphirine or orthopyroxene became partially or completely entrapped within garnet, effectively creating varied sets of subassemblages. As *P–T* conditions continued to change and garnet was consumed, the diverse sets of reaction textures, some of which are illustrated in Fig. 3, developed in the local compositional domains within the garnets and at and around the garnet grain boundaries.

Reaction textures are so well preserved in these rocks that individual thin sections commonly show a spectrum of textures (i.e. Fe–Mg continuous reactions that did not run to completion). Using numerous thin sections, we have been able to reconstruct the approximate sequence of reactions.

FeO–MgO–Al_2O_3–SiO (FMAS) reactions

Most of the phases that are involved in producing the reaction textures can be described by FMAS components. These reactions bound the permissible *P–T* conditions of additional phase equilibria in systems with additional components (e.g. FMAS + H_2O, Na_2O or CaO) and phases. Consequently, the sequence of FMAS phase relations provides a basic framework into which the more complex phase relations must logically fit, if our interpretations of the FMAS reaction textures and their relative timing are correct. Figure 5 and the following discussion outline the basic FMAS phase relations that are based on the textural observations. Explanations of the phase relations and timing of minerals with additional components (e.g. gedrite and plagioclase) are discussed subsequently.

Garnet growth and resorption in corundum-bearing assemblages (Munwatte)

The most striking textures at the Munwatte locality are the zoned sets of assemblages within the large garnets (see Fig. 3a and earlier discussion). These assemblages can be explained by three Fe–Mg continuous reactions and are the earliest reactions preserved in these rocks.

Thin sapphirine rims on some of the matrix spinel may have formed by the reaction

$$\text{Opx} + \text{Sp} + \text{Cor} = \text{Spr} \ [\text{low } P, \text{ high } T]$$

[where the text in square brackets indicates the pressure and temperature of the right-hand side of the reaction (see Tables 9 and 10, below)] (see Fig. 3b). [Determining the reaction that caused the sapphirine overgrowths of spinel that are outside of the garnets (Fig. 3b) is not straightforward. An alternative possibility is the continuous Fe–Mg reaction

$$\text{Sp} + \text{Gar} = \text{Spr} + \text{Opx} \ [\text{low } P, \text{ low } T].$$

This reaction would have followed garnet growth. It cannot be shown in any of the projection schemes, but would have been stable at the conditions of Fig. 5c–m (+ Cor) (between the Crd and Cor-absent reactions of the [Qz, Sil] invariant point, Fig. 6). All the phases necessary for reaction (4) are present in the vicinity and sapphirine completely encloses the spinel; however, the textures do not conclusively demonstrate the involvement of the garnet rims. Consequently, reaction (1) is favoured.]

The presence of orthopyroxene (Opx) + spinel (Sp) in the matrix and spinel + corundum (Cor) as relicts in the garnet interiors suggests that garnet grew via the reaction

$$\text{Opx} + \text{Cor} = \text{Gar} \ [\text{high } P, \text{ high } T]$$

which, because of a compositional degeneracy within the FMAS system, plots as a linear two-phase field rather than a three-phase field on the corundum projection in Fig. 5a.

The textures (Fig. 3a) clearly indicate the production of sapphirine from garnet, corundum and spinel. These four phases cannot coexist at the conditions of Fig. 5a and require that the univariant boundary

$$\text{Opx} + \text{Sp} + \text{Cor} = \text{Spr} + \text{Gar} \ [\text{high } P, \text{ high } T]$$

be crossed (Fig. 5b). At the conditions of (Fig. 5c), the continuous Fe–Mg reaction

$$\text{Sp} + \text{Gar} + \text{Cor} = \text{Spr} \ [\text{low } P, \text{ high } T]$$

produced the sapphirine that isolates spinel + corundum from garnet in the Munwatte samples.

Garnet growth in quartz- or sillimanite-bearing assemblages (Hakurutale)

Indications of the earliest reaction assemblages are found in the garnets. The garnet cores enclose large prismatic orthopyroxene, sillimanite and, locally, coarse sapphirine. The coarse orthopyroxene and sillimanite are also found in the matrix, but not the sapphirine. At and near the

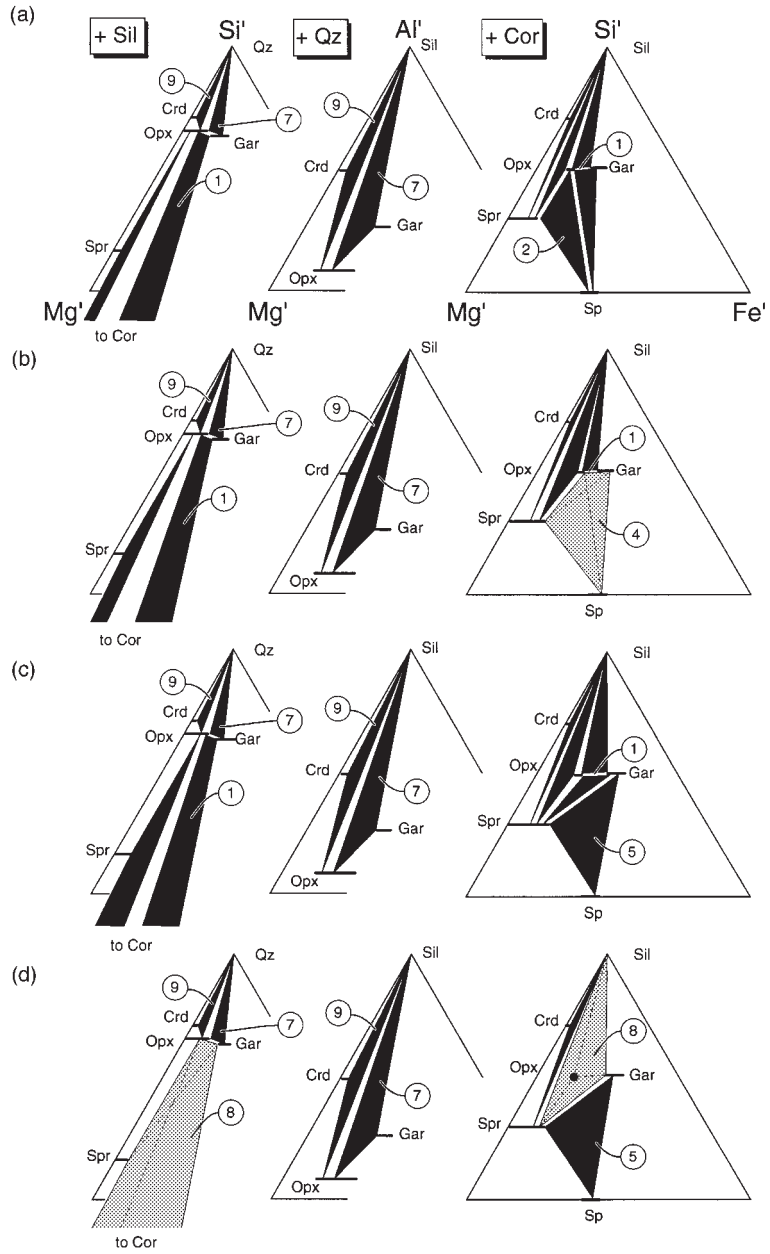

Fig. 5. (a–d).

garnet rims sapphirine gives way to quartz. This crude spatial arrangement of phases is consistent with the following two continuous Fe–Mg reactions:

$$\text{Spr} + \text{Opx} + \text{Sil} = \text{Gar} \text{ [high } P\text{, low } T\text{]}$$

followed by

$$\text{Opx} + \text{Sil} = \text{Gar} + \text{Qz} \text{ [high } P\text{, high } T\text{]}$$

both of which are stable at the conditions represented by Fig. 5e. This implies crossing of the univariant boundary

$$\text{Opx} + \text{Cor} = \text{Spr} + \text{Sil} + \text{Gar} \text{ [low } P\text{, high } T\text{]}.$$

The implications are that garnet grew in the presence of sapphirine + orthopyroxene + sillimanite; sapphirine either reacted away or was isolated from orthopyroxene and sillimanite within garnet. Orthopyroxene and sillimanite then continued to react and produced quartz and additional garnet. This texture as well as this scenario suggests that, although sapphirine and quartz are present in the same thin section, they were not an equilibrium assemblage.

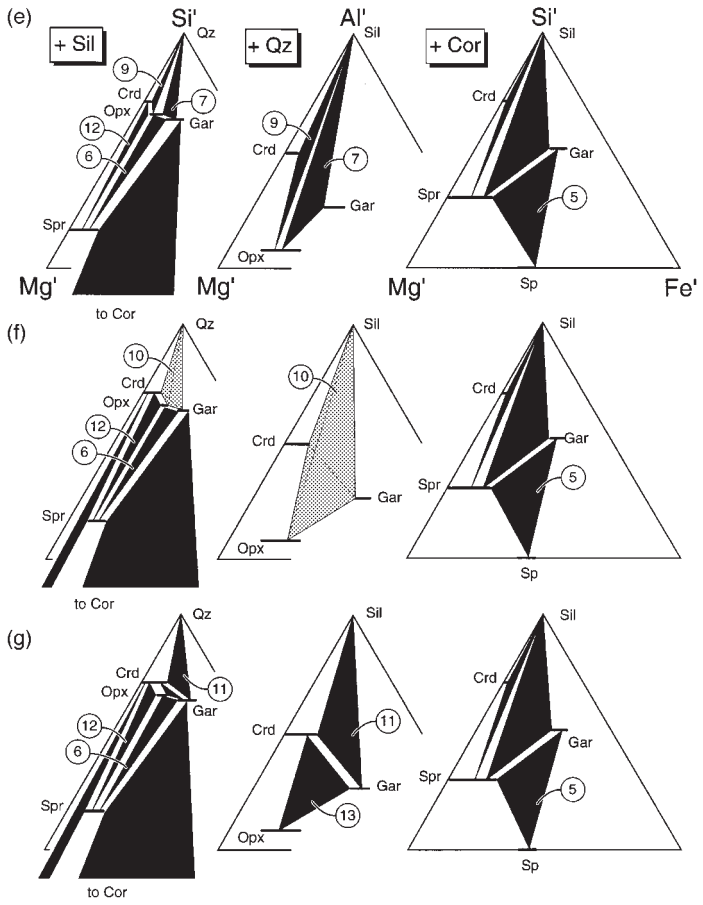

Fig. 5. (e–g).

Decompression reaction textures

In the rims of some garnets, symplectitic intergrowths of orthopyroxene and sillimanite separate garnet and quartz, suggesting that reaction (7) was recrossed (Fig. 5a–f). This reaction rarely occurs in garnet interiors, but is ubiquitous at the outer rim of garnet, which suggests that it was possibly catalysed by the presence of fluid or that the garnet, acting like a pressure vessel, was strong enough to hinder the reaction in the garnet cores. In the core, garnet locally breaks down to a symplectitic intergrowth of orthopyroxene, sillimanite and sapphirine, indicating the partial reverse of reaction (6) (Fig. 5e–g). This apparent reversal of both continuous reactions (6) and (7) at Hakurutale implies a change in slope of the P–T path.

At Munwatte, this same reaction seems to have occurred very locally. Small prismatic grains of orthopyroxene, sillimanite and sapphirine [reaction (6), Fig. 5e–g) have also been observed in fractures in garnet (Fig. 3c), and their formation post-dates the reactions involving corundum that were discussed previously. This is an important observation because it is the earliest point at which the reaction sequences at both localities can be correlated.

Cordierite is texturally later at both localities but is more extensively developed at Hakurutale. Cordierite separates orthopyroxene, sillimanite and quartz, and encloses quartz at the garnet rim areas, which suggests the reaction

$$\text{Opx} + \text{Sil} + \text{Qz} = \text{Crd} \ [\text{low } P, \text{ high } T]$$

which can occur at the same conditions as reaction (7) in domains richer in Mg (Fig. 5a–e). The textures also suggest that garnet reacts with sillimanite $\pm$ quartz at Hakurutale to form cordierite (Fig. 3d–f). These reactions indicate continuing change of the metamorphic conditions and that the univariant boundary

$$\text{Opx} + \text{Sil} + \text{Qz} = \text{Crd} + \text{Gar} \ [\text{low } P, \text{ high } T]$$

was crossed (Fig. 5f). At Hakurutale, where cordierite separates garnet from sillimanite and quartz, one of the newly stable continuous Fe–Mg reactions is

$$\text{Gar} + \text{Sil} + \text{Qz} = \text{Crd} \ [\text{low } P, \text{ high } T].$$

Also at Hakurutale, towards the garnet cores, sillimanite

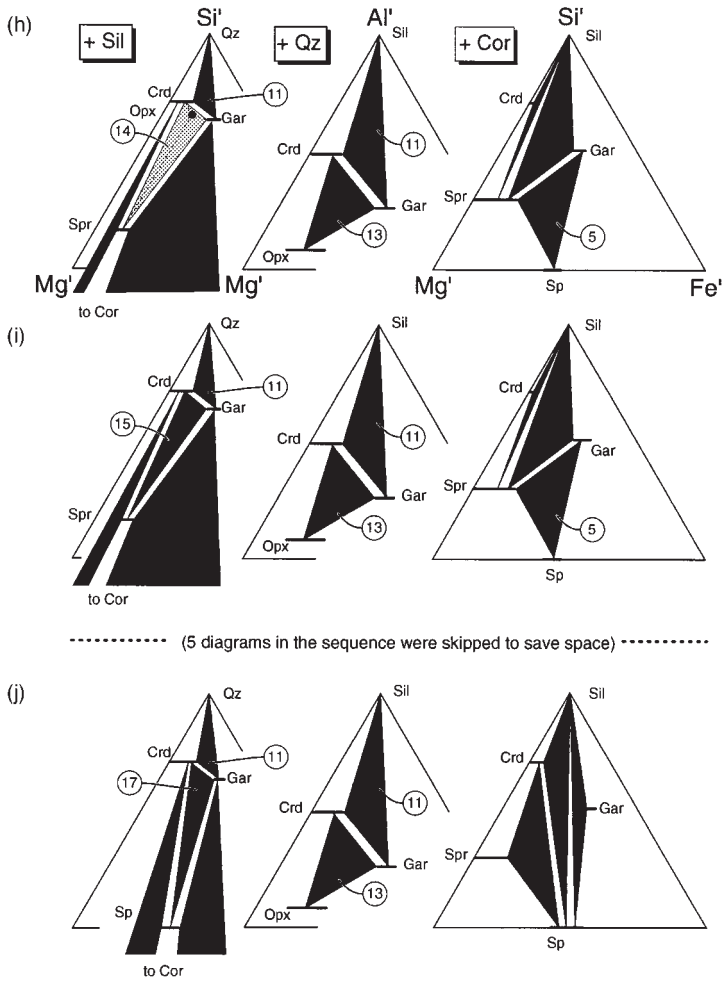

Fig. 5. Projections from sillimanite (+ Sil), quartz (+ Qz) and corundum (+ Cor) to various ternary planar sections within an FeO–MgO–Al_2O_3–SiO_2 tetrahedron (see Robinson & Jaffe, 1969; Schumacher & Robinson, 1987). The diagrams show an idealized progression of discontinuous and continuous reactions that correspond to the sequence and identity of reactions seen in samples that were used in the present study. Numbers enclosed in circles are reaction numbers used in the text and in other figures; filled polygonal areas are three-phase fields corresponding to the continuous Fe–Mg reaction assemblages; grey polygonal areas are four-phase fields corresponding to the discontinuous Fe–Mg reaction assemblages. Crd, cordierite; Spr, sapphirine; Opx, orthopyroxene; Sp, spinel; Gar, garnet. In Sil projections: Si′ represents SiO_2 + MgO + FeO–Al_2O_3; Mg′, MgO; Fe′, FeO. In Qz projections: Al′, Al_2O_3; Mg′, MgO; Fe′, FeO. In Cor projections: Si′, SiO_2; Mg′, MgO; Fe′, FeO. (All coordinates in moles.)

is separated from orthopyroxene by a symplectitic intergrowth of cordierite and sapphirine, indicating the reaction

$$\text{Opx} + \text{Sil} = \text{Crd} + \text{Spr} \text{ [low } P\text{, high } T\text{]}$$

(Fig. 5e–g). Similar cordierite + sapphirine symplectites are found at the Munwatte locality.

Garnet and quartz are also separated by coronas and symplectitic intergrowths of orthopyroxene and cordierite (Fig. 3g, Hakurutale), suggesting that further garnet + quartz breakdown via

$$\text{Gar} + \text{Qz} = \text{Crd} + \text{Opx} \text{ [low } P\text{, high } T\text{]}$$

occurred (Fig. 5g–j). Orthopyroxene–cordierite symplectites without relict quartz are common in the Munwatte samples, and these symplectites suggest that quartz was completely consumed in the reaction.

In the quartz-free core areas of garnets from the Hakurutale locality, sillimanite is separated from garnet by a symplectitic intergrowth of sapphirine and cordierite, which suggests that another univariant reaction,

$$\text{Opx} + \text{Sil} = \text{Crd} + \text{Spr} + \text{Gar} \text{ [low } P\text{, high } T\text{]}$$

was crossed (Fig. 5h). One of the newly stable continuous Fe–Mg reactions,

$$\text{Gar} + \text{Sil} = \text{Crd} + \text{Spr} \text{ [low } P\text{, high } T\text{]}$$

(Fig. 5i) explains the observed cordierite + sapphirine symplectite.

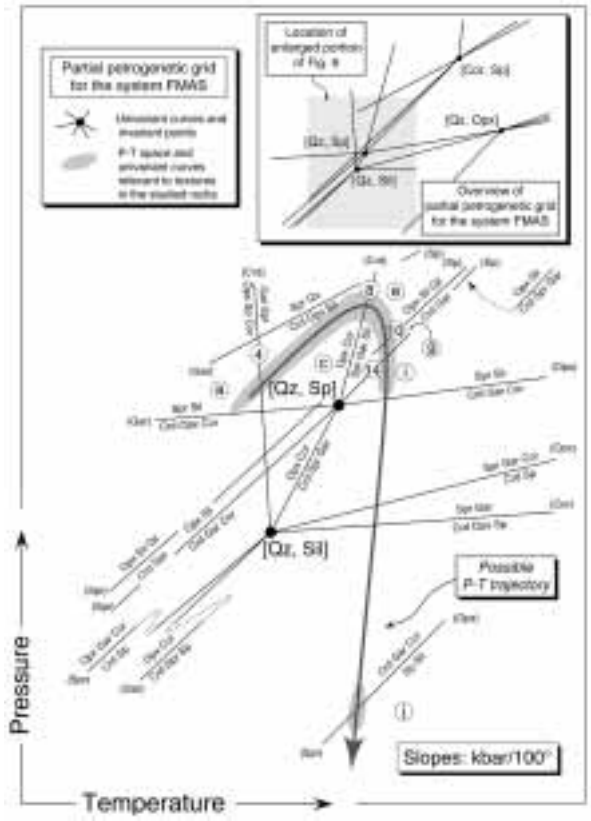

Fig. 6. Partial petrogenetic grid for ideally discontinuous reactions involving cordierite (Crd), sapphirine (Spr), orthopyroxene (Opx), spinel (Sp), garnet (Gar), sillimanite (Sil), quartz (Qz) and corundum (Cor) in the FeO–MgO–Al_2O_3–SiO_2 (FMAS) system. Phase compositions, reaction stoichiometry and other information that was used in the construct of the diagram are given in Tables 9 and 10. Square brackets indicate phases absent at the invariant point and parentheses indicate the additional phase that is absent along each univariant curve. Each upper case letter that is enclosed in a circle indicates the identity of the phase diagram set from Fig. 5 that describes the phase relations of the labelled P–T field. (See text for discussion.)

Additionally, at Hakurutale, in the garnet core regions, away from quartz, garnet breaks down to an orthopyroxene–cordierite ± sapphirine symplectite, in which sapphirine and orthopyroxene are commonly intergrown. This suggests a quartz-absent garnet breakdown by the continuous Fe–Mg reaction

$$\text{Gar} = \text{Crd} + \text{Spr} + \text{Opx} \text{ [low } P\text{, high } T\text{]}.$$

This reaction cannot be represented in the projections of Fig. 5. The textural relations suggest that reaction (16) occurred simultaneously with or after reaction (15) and reaction assemblage (16) could be stable over the range of conditions represented by ternary i (Fig. 5) (bounded by the Cor- and Sil-absent curves of the [Qz, Sp] invariant point and the Cor-absent curve of the [Qz, Sil] invariant point, Fig. 6).

Orthopyroxene–sapphirine symplectites are also found at the rims of both garnet and prismatic orthopyroxene. A possible genesis is a retrograde exsolution of highly aluminous orthopyroxene, analogous to the exsolution of orthopyroxene from sapphirine described by Seifert *et al.* (1992). They have also been observed at the contact of garnet and orthopyroxene inclusions, suggesting a possible retrograde re-equilibration of Al in orthopyroxene with the contiguous garnet.

In places, at the garnet rims in the Hakurutale samples, very small (0·07 mm) spinel grains are locally present in cordierite rims separating sillimanite from garnet. Reaction textures are not as clear as those discussed above, but the presence of nearby garnet suggests

$$\text{Gar} + \text{Sil} = \text{Crd} + \text{Sp} \text{ [low } P\text{, high } T\text{]}$$

(Fig. 5j) as a plausible spinel-forming reaction. (At least five sets of additional compatibility diagrams are necessary to derive Fig. 5j from Fig. 5i.)

Breakdown of the assemblage garnet + sillimanite via reaction (17) certainly occurred later than via reaction (15), possibly because the garnet that was consumed had a lower X_{Mg}. Alternatively, the rare occurrence of spinel could be explained by the stabilizing effect of ZnO on spinel although the ZnO contents of the spinels are low (Table 6).

Most of these reactions discussed have been reported earlier in the literature. In particular, Droop & Bucher-Nurminen (1984) and Bertrand *et al.* (1992) have described similar textures and complex reaction sequences for high-T granulites in the Alps and North Africa, respectively. However, unlike in many other sapphirine localities, the textures described here document the parallel development of reaction sequences in quartz-free and quartz-bearing granulites.

Reactions in plagioclase-bearing assemblages

Although rarer, plagioclase is found in some assemblages. The reactions involving plagioclase resemble those modelled above using the FMAS system components. In these assemblages, CaO becomes an additional important system component, and, as only two CaO-bearing phase components are present, any CMASH reactions will have the anorthite component of the plagioclase on one side and the grossular component of the garnet on the other. These reactions do not provide new definitive information concerning the P–T trajectory, but they do allow better constraints on the P–T estimates (see below).

Munwatte

In some thin sections from Munwatte, intergrowths of sapphirine and plagioclase form composite inclusions in

garnet (Fig. 3i), which suggests equilibria involving the grossular component of Ca–Fe–Mg garnet (Gar_{ss}). A possible mechanism for generating this texture is by reaction

$$Cor + Gar_{ss} = Spr + Plg.$$

In corundum-free parts of these samples, plagioclase also appears to have been produced locally in CFMAS versions of garnet breakdown reactions (7), (11) and (13); however, quartz is not present and its former presence is only tentatively inferred from the reaction stoichiometry.

Hakurutale

Plagioclase is rarely enclosed by garnet in the Hakurutale samples, where it could be involved in CFMAS equivalents of garnet-producing reactions (5) and (6):

$$Spr + Opx + Sil + Plg = Gar_{ss}$$

followed by

$$Opx + Sil + Plg = Gar_{ss} + Qz.$$

Where plagioclase is present, it normally occurs as a product phase in orthopyroxene–sillimanite and orthopyroxene–cordierite symplectites and in cordierite coronas formed by garnet breakdown via CFMAS analogues of the reactions (7), (9), (11) and (13). Locally, plagioclase is associated with orthopyroxene only in coronas separating garnet from quartz, which suggests the reaction

$$Gar_{ss} + Qz = Opx + Plg$$

a reaction that is widespread in the metamorphosed basic rocks of Sri Lanka (Schenk *et al.*, 1988; Schumacher *et al.*, 1990; Faulhaber & Raith, 1991).

FMAS PETROGENETIC GRIDS: CONSTRAINTS ON *P–T* TRAJECTORY

Several petrogenetic grids have been proposed for the FMAS system comprising the phases cordierite, sapphirine, orthopyroxene, spinel, garnet and sillimanite, in combination with either quartz (Hensen, 1971, 1986; Vielzeuf, 1983; Waters, 1986) or corundum (Hensen, 1987). All these grids employ semi-quantitative methods, because the thermodynamic data for some phases, notably sapphirine, are insufficient to warrant a rigorous treatment. In the MAS end member system, phase relations are better known (e.g. Schreyer & Seifert, 1969).

Plotting the divariant assemblages described earlier in the order of appearance on any of these grids results in a clockwise *P–T* path (*P*-axis vertical) for the Hakurutale and Munwatte samples. However, some inconsistencies become apparent in detail. For example, some of the univariant boundaries that are crossed do not appear in all of these grids, whereas it follows from the grids that other lines should have been crossed but were not recorded.

In an attempt to work out these inconsistencies, a new partial petrogenetic grid has been constructed for the phases cordierite, sapphirine, orthopyroxene, spinel, garnet, sillimanite, corundum and quartz from ideal mineral compositions that as closely as possible reflect the Fe–Mg ratios and, where applicable, the extent of the Tschermaks-type substitution of the measured compositions (Table 8). Estimates of volume and rough estimates of entropy at 25°C were extrapolated from data given by Berman (1988), Holland (1989) and Massonne (1992). Balanced reactions were used to calculate the ΔV and ΔS at 25°C ($\Delta C_p = 0$) of reaction for univariant curves and the orientations of the continuous reactions (Tables 9 and 10) which are shown in Figs 6, 7a and 8a. As a further check on the validity of these *P–T* slopes at elevated *P* and *T*, the orientations of the sapphirine- and spinel-free reactions were calculated at *P* and *T* using the 1992 revision of the data of Berman (1988), ideal site mixing models for Fe–Mg end members of orthopyroxene and cordierite, the Berman (1990) mixing model for Fe–Mg garnet and the PERPLEX software of Connolly (1990). Comparisons of Fig. 7a and b as well as Fig. 8a and b indicate extremely good agreement among all the orientations of the common sapphirine- and spinel-absent univariant and divariant curves. Provided that the sapphirine values are realistic, then Figs 7a and 8b should give a good approximation of the phase relations for these bulk compositions in this part of *P–T* space.

The *P–T* orientations of the continuous reactions in Figs 7a and 8a agree reasonably well with analogous reactions in the end member $MgO–Al_2O_3–SiO_2$ system. Additionally, the orientations of many of the FeO–$MgO–Al_2O_3–SiO_2$ univariant curves in Figs 7a and 8a have similar orientations to those found in the literature (e.g. Waters, 1986; Hensen & Harley, 1990; Bertrand *et al.*, 1991, 1992; note that the orientations of the univariant curves in these petrogenetic grids do not agree completely with one another) whereas other curves depart markedly. Lack of agreement among published petrogenetic grids for these assemblages has also been noted by Regan & Stout (1992), who have reported an attempt to constrain the topology of quartz-free, $FeO–MgO–Al_2O_3–SiO_2$, univariant reactions with calculations based on thermodynamic data for these phases (unfortunately the dataset was not identified by those workers). Some of this lack of consistency is related to the uncertainties associated with the thermodynamic data of sapphirine.

In this study, Mg–Al end member data for sapphirine that were recently reported by Massonne (1992) and were derived with data from Berman (1988) were used

Table 8: Compositions and entropy (S_{ideal}) and volume (V_{ideal}) data that were used to calculate FMAS discontinuous and continuous reactions given in Tables 9 and 10

Mineral	Formula	S_{ideal}	V_{ideal}	Key
Orthopyroxene	$Mg_2Si_2O_6$	132·340	6·266	B
	$FeMg_{-1}$	29·712	0·163	B
	$AlAlMg_{-1}Si_{-1}$	−1·749	−0·264	a
	$Fe_{0\cdot38}Mg_{1\cdot52}Al_{0\cdot10}Si_{1\cdot90}Al_{0\cdot10}O_6$	155·054	6·305	b
Garnet	$Mg_3Al_2Si_3O_{12}$	266·359	11·316	B
	$FeMg_{-1}$	24·523	0·065	B
	$Fe_{1\cdot2}Mg_{1\cdot8}Al_2Si_3O_{12}$	312·573	11·433	c
Cordierite	$Mg_2Al_4Si_5O_{18}$	417·970	23·311	B
	$FeMg_{-1}$	17·543	0·198	B
	$Fe_{0\cdot15}Mg_{1\cdot85}Al_4Si_5O_{18}$	425·031	23·677	d
Spinel	$MgAl_2O_4$	84·535	3·977	B
	$FeMg_{-1}$	22·478	0·098	B
	$Fe_{0\cdot3}Mg_{0\cdot7}Al_2O_4$	96·357	4·046	e
Sapphirine	$[Mg_4Al_4][Al_4Si_2]O_{20}$	430·000	19·733	M
	$[Mg_3Al_5][Al_5Si_1]O_{20}$	422·000	19·530	M
	$[Mg_{3\cdot5}Al_{4\cdot5}]\ [Al_{4\cdot5}Si_{1\cdot5}]O_{20}$	434·644	19·632	f, M
	$FeMg_{-1}$	29·712	0·163	g
	$Fe_{0\cdot35}Mg_{3\cdot15}Al_{4\cdot50}Si_{1\cdot50}Al_{4\cdot50}O_{20}$	454·503	19·689	h
Sillimanite	Al_2SiO_5	95·930	4·983	B
α Quartz	SiO_2	41·460	2·269	B
Corundum	Al_2O_3	50·820	2·558	B
$FeMg_{-I}$		25·217	0·179	i,B

Estimates of volume and of entropy at 25°C were extrapolated from data given by Berman (1988) and Massonne (1992). Equations that were used for ideal entropy and volume calculations: $\bar{V}_{ideal} = \Sigma_i X_i \bar{V}_i$ and $\bar{S}_{ideal} = \Sigma_i X_i \bar{S}_i - nR\Sigma X_i \ln X_i$. Key: B, Berman (1988) data (Jun92.rgb version); M, Massonne (1992) data (derived with Berman data); a, based on data of Berman (1988) for $CaAl_2SiO_6$–diopside exchange; b, molecular model, local charge balance, ideal mixing on *M1* and X_{Mg} at *MI* = X_{Mg} at *M2*; c, molecular model, local charge balance, ideal mixing on the 3Fe–Mg sites; d, ideal mixing on the 2Fe–Mg sites; e, molecular model, ideal mixing on 1Fe–Mg sites; f, molecular model, local charge balance, ideal mixing on one site; g, taken from orthopyroxene; h, molecular model, ideal mixing on the 3·5Fe–Mg sites; i, S is an average from ferrosilite–enstatite, hedenbergite–diopside, Fe-cordierite–cordierite, hercynite–spinel and almandine–pyrope exchanges. *V* is an average from ferrosilite–enstatite, hedenbergite–diopside, Fe-cordierite–cordierite exchanges.

in an attempt to orient the univariant curves that involve sapphirine. It is not the purpose of the present work to resolve these inconsistencies among various petrogenetic grids; nevertheless, we feel that the sequence of assemblages that are suggested by the textures and array of reaction curves derived from these data support the *P–T* trajectory that is derived from the petrogenetic grids given below.

The reaction sequence that was outlined above (Fig. 5) traces a roughly clockwise (i.e. P_{max} before T_{max}) *P–T* trajectory through the univariant curves and divariant *P–T* regions in Fig. 6. The divariant *P–T* regions (Fig. 6) are labelled with upper case letters that correspond to the lettered composition phase diagrams in Fig. 5, and the lighter grey regions that highlight the *P–T* trajectory (arrow) denote the *P–T* areas where the garnet- and corona-forming reactions could have occurred.

As is evident from Fig. 5, each of the ideally univariant curves (assemblages) is associated with a set of divariant Fe–Mg continuous reactions. The *P–T* fields where the continuous reactions occur are bounded by these univariant curves. Each continuous reaction within the *P–T* fields can be represented as a family of reaction curves, each representing a set of equilibrium Fe–Mg compositions for the phases of the continuous reaction. Using the data in Table 8, examples of the slopes of the continuous reactions that produced the corona textures and inclusion assemblages were calculated and are shown along with some of the associated univariant curves from Fig. 6 in Figs 7a and 8a (circled numbers identify reactions discussed in the text and illustrated in Fig. 5).

As discussed earlier, the continuous reaction (2) is compositionally degenerate and is stable on both sides of the univariant curve (4), but it terminates on the high-

Table 9: FMAS discontinuous reactions that were used to construct Fig. 6 and parts of Figs 7 and 8.

IP/RN	Reaction stoichiometry								Reaction properties		
	Opx	Gar	Crd	Spr	Sp	Sil	Qz	V	ΔV (J/bar)	ΔS (J/°C)	$\Delta S/\Delta V$ (kbar/100°C)
[Cor, SP]											
(Opx)	0	−0·011	−0·201	0·125	0	−0·147	1	0	−0·887	−4·698	0·530
(Gar)	−0·047	0	−0·178	0·127	0	−0·212	1	0	−0·798	−4·098	0·695
(Crd)	−0·406	0·086	0	0·147	0	−0·706	1	0	0·069	4·475	6·506
(Spr) (10)	2·267	−0·552	−1·326	0	0	2·977	1	0	−6·310	−57·579	0·913
(Sil)	0·107	−0·037	−0·254	0·119	0	0	1	0	−1·150	−7·386	0·642
(Qz) (14)	0·726	−0·173	−0·360	−0·040	0	1	0	0	−1·729	−16·767	0·970
[Qz, Opx]											
(Gar)	0	0	0·214	−0·137	0·053	−0·863	0	1	0·842	1·829	0·217
(Crd)	0	0·192	0	0·082	−0·863	−0·699	0	1	−0·607	−2·108	0·347
(Spr)	0	0·120	0·080	0	−0·520	−0·760	0	1	−0·067	−0·981	1·022
(sp)	0	0·011	0·201	−0·125	0	−0·853	0	1	0·731	1·048	0·143
(Sil)	0	1·009	−0·911	1·018	−4·768	0	0	1	−6·722	−17·744	0·264
(Cor)	0	1·170	−1·304	1·339	−5·589	1	0	0	−8·762	−22·561	0·258
(Opx)	0	0·011	0·201	−0·125	0	−0·853	0	1	0·731	1·048	0·143
(Gar)	0·047	0	0·178	−0·127	0	−0·788	0	1	0·642	0·448	0·699
(Crd) (8)	0·406	−0·086	0	−0·147	0	−0·294	0	1	−0·225	−8·215	3·615
(spr)	−2·267	0·552	1·326	0	0	−3·977	0	1	6·154	53·929	0·876
(Sil)	0·619	−0·137	−0·106	−0·159	0	0	0	1	−0·746	−13·343	1·789
(Cor) (14)	0·726	−0·173	−0·360	−0·040	0	1	0	0	−1·729	−16·767	0·970
[Qz, Sill]											
(Opx)	0	1·009	−0·911	1·018	−4·768	0	0	1	−6·722	−17·744	0·264
(Gar)	0·545	0	−0·202	−0·018	−0·569	0	0	1	−1·445	−13·540	0·937
(Crd) (4)	0·701	−0·287	0	−0·313	0·626	0	0	1	0·066	−12·135	−18·308
(Spr)	0·536	0·018	−0·214	0	−0·643	0	0	1	−1·525	−13·359	0·876
(Sp)	0·619	−0·137	−0·106	−0·159	0	0	0	1	−0·746	−13·343	1·789
(Cor)	0·130	−0·240	0·169	−0·247	1	0	0	0	1·260	1·065	0·095

Sums of of all reactions are zero. Crd, cordierite; Spr, sapphirine; Opx, orthopyroxene; Sp, spinel; Gar, garnet; Sil, sillimanite; Qz, quartz; Cor, corundum. IP, invariant point designation shown with square brackets; RN, reaction number used in text and in figures; otherwise the phase that is absent from the reaction is shown with parentheses.

pressure side of the univariant curve Opx + Cor = Spr + Gar + Sil (Fig. 8). This configuration of reaction curves indicates that the prograde *P–T* path would have had to lie at lower *T* and/or higher *P* than the [Qz, Sp] and [Qz, Sil] invariant points whereas the decompression part of the *P–T* trajectory must have passed these invariant points at higher *T*. This scenario both fits the observed reaction sequence and explains the manner in which back-reaction of the garnet to orthopyroxene and corundum was avoided.

The orientations of the continuous reactions that are relevant to the textures which formed at Hakurutale and Munwatte are displayed in Figs 7 and 8. As with the univariant curves (Fig. 6), the orientation and sequence of the continuous reactions suggest that the *P–T* trajectory was 'clockwise'. Crossing the garnet-forming reactions at high angles suggests a prograde *P–T* path dominated by a heating component; whereas the corona-forming stage was dominantly a decompressional event. Unfortunately, these rocks do not record either the extent or nature of the *P–T* trajectory between the garnet- and corona-forming stages (queried, broken part of the *P–T* path in Figs 7 and 8). The simplest interpretation is that the *P–T* trajectory undergoes a simple, knee-shaped change in

Table 10: FMAS continuous reactions that were used to construct parts of Figs 7 and 8

Reaction no.	Reaction stoichiometry								Reaction properties		
	Opx	Gar	Crd	Spr	Sp	Sil	Cor	$FeMg_{-1}$	ΔV (J/bar)	ΔS (J/°C)	$\Delta S/\Delta V$ (kbar/100°C)
(1)	−2·632	1·667	0	0	0		−1·404	−1	−1·306	16·387	−1·255
(2)	1·435	0	0	−1·818	3·636	0	4·402	−1	−0·956	−54·936	5·746
(3)	−1·648	1·264	0	−0·440	0·879	0	0	−1	−1·225	−0·938	0·077
(5)	0	0·588	0	−1·176	2·353	0	2·353	−1	−1·072	−29·612	2·761
(6)	−2·062	1·546	0	−0·206	0	−0·412	0	−1	−1·613	5·147	−0·319
(7)	−2·632	1·667	0	0	0	−1·404	1·404	−1	−1·525	11·262	−0·739
(9)	4·211	0	−4·000	0	0	7·579	4·421	−1	−20·540	−162·059	0·789
(11)	0	1·026	−1·538	0	0	2·051	2·564	−1	−8·826	−55·159	0·625
(12)	4·418	0	−3·213	−0·562	0	8·514	0	−1	−17·039	−144·494	0·848
(13)	−1·563	1·406	−0·625	0	0	0	1·875	−1	−4·505	−15·997	0·355
(15)	0	1·054	−1·022	−0·319	0	2·428	0	−1	−6·509	−42·216	0·649
(16)	−1·763	1·475	−0·148	−0·223	0	0	0	−1	−2·326	−1·792	0·077
(17)	0	1·333	−1·333	0	−1·333	2·667	0	−1	−8·603	−47·723	0·555

Sums of of all reactions are zero. Crd, cordierite; Spr, sapphirine; Opx, orthopyroxene; Sp, spinel; Gar, garnet; Sil, sillimanite; Qz, quartz; Cor, corundum; $FeMg_{-1}$, Fe–Mg exchange component.

orientation; however, data from the metamorphosed basic rocks that were not part of this study suggest possible alternatives, and these are explored in later discussion.

REACTIONS THAT INVOLVE OR MAY INVOLVE A FLUID PHASE

The reactions and their sequence as outlined above account for the vast majority of textures and assemblages found at the Hakurutale and Munwatte localities. Nevertheless, some observations, such as the presence of texturally later gedrite or the development of Spr + Crd at some but not all Sil–Opx grain boundaries on the thin-section scale, necessitate additional explanation.

The presence of rare F-bearing gedrite as inclusions in texturally later sapphirine suggests that a fluid phase was at least locally present as the reactions proceeded. Further, the stability of cordierite is strongly influenced by the incorporation of channel fluids. Consequently, by implication, local availability of fluid could play a crucial role in catalysing reactions that produce cordierite. Although reaction kinetics plays a role, to a first approximation, local variation at the thin-section scale in the amounts of a fluid phase that is available coupled with 'metamorphic fractionation' of components of the fluid phase can explain the observations.

Gedrite inclusions in sapphirine

At the Munwatte locality, tiny blebs of gedrite, which were not included in the model FMAS reactions given above, are also present only within the sapphirine, which is (1) a relict of an earlier amphibolite-facies assemblage or (2) late reaction product associated with sapphirine formation. Late production of gedrite is favoured for the following reason. If the gedrites were relicts, then they must have formed at lower temperature. Common assemblages for bulk compositions like those at Hakurutale and Munwatte at amphibolite-facies conditions are gedrite + aluminosilicate ± cordierite ± garnet (Robinson & Jaffe, 1969; Spear, 1982; Schumacher & Robinson, 1987). At lower temperature, gedrites tend to be dominantly OH-amphiboles (poor in F and Cl). In contrast, the Munwatte gedrites have a significant F content, suggesting to us that they formed from an H_2O-poor, multicomponent fluid, which is more consistent with fluids in granulites.

A more probable origin for the gedrite is that it was stabilized by the presence of minute amounts of a multicomponent fluid phase as the sapphirine formed.

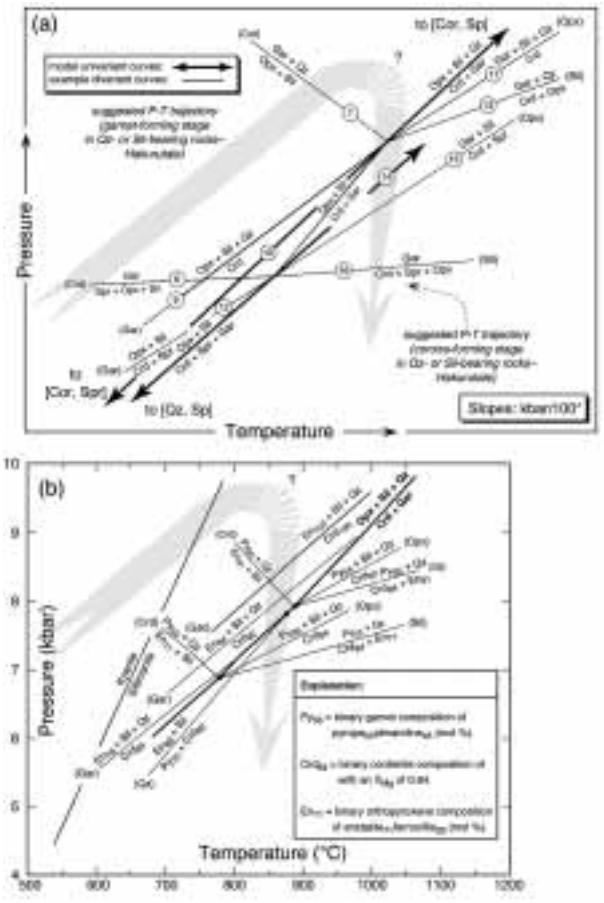

Fig. 7. (a) Partial petrogenetic grid for the FeO–MgO–Al_2O_3–SiO_2 (FMAS) system showing the *P*–*T* orientations of continuous Fe–Mg reactions that involve cordierite (Crd), sapphirine (Spr), orthopyroxene (Opx), garnet (Gar), sillimanite (Sil) and quartz (Qz), and lie around two univariant assemblages. The reactions portrayed in this diagram are relevant to the Hakurutale locality. Phase compositions, reaction stoichiometry and other information that was used in the construction of the diagram are given in Tables 9 and 10. Parentheses indicate the additional phase that is absent along each continuous reaction curve. The numbers enclosed in circles indicate reaction numbers used in the text and on other figures. (See text for discussion.) (b) *P* and *T* orientations of one univariant curve and selected Fe–Mg isopleths for sapphirine- and spinel-free continuous reactions from (a). These were calculated with the PERPLEX software of Connolly (1990) and used the 1992 revision of the data of Berman (1988), ideal site mixing models for Fe–Mg end members of orthopyroxene and cordierite, and the Berman (1990) mixing model for Fe–Mg garnet.

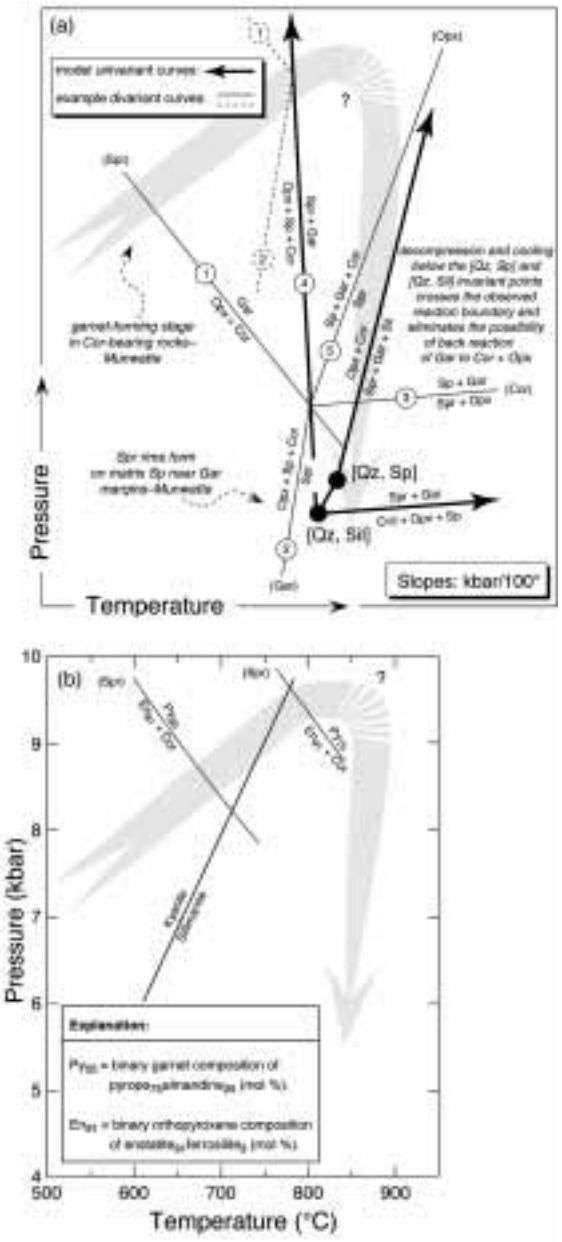

Fig. 8. Partial petrogenetic grid for the FeO–MgO–Al_2O_3–SiO_2 (FMAS) system showing the *P*–*T* orientations of continuous Fe–Mg reactions that are relevant to the Munwatte locality and involve sapphirine (Spr), orthopyroxene (Opx), spinel (Sp), garnet (Gar) and corundum (Cor), and lie around two univariant assemblages. The two dashed curves indicate the possible alternative positions of the reactions for different Fe–Mg bulk compositions. Phase compositions, reaction stoichiometry and other information that was used in the construction of the diagram are given in Tables 9 and 10. Parentheses indicate the additional phase that is absent along each continuous reaction curve. The numbers enclosed in circles indicate reaction numbers used in the text and in other figures. (See text for discussion.) (b) *P* and *T* orientations of two Fe–Mg isopleths and the continuous reaction that produces garnet from orthopyroxene and corundum from (a). These were calculated with the PERPLEX software of Connolly (1990) and used the 1992 revision of the data of Berman (1988), ideal site mixing models for Fe–Mg end members of orthopyroxene and the Berman (1990) mixing model for Fe–Mg garnet.

Assuming that small amounts of a multicomponent fluid phase were locally present, the relation of gedrite production to the sapphirine-forming reaction (5) can be illustrated and modelled on a (*P*–*T*-path)–μ_{Fluid} diagram (Fig. 9) with 'Fluid' representing an H_2O–F-bearing multicomponent fluid that may have stabilized the gedrite. The two arrows (paths I and II, Fig. 9) in the (*P*–*T*-path)–μ_{Fluid} diagram represent schematically the paths followed by two local bulk compositions, one with very

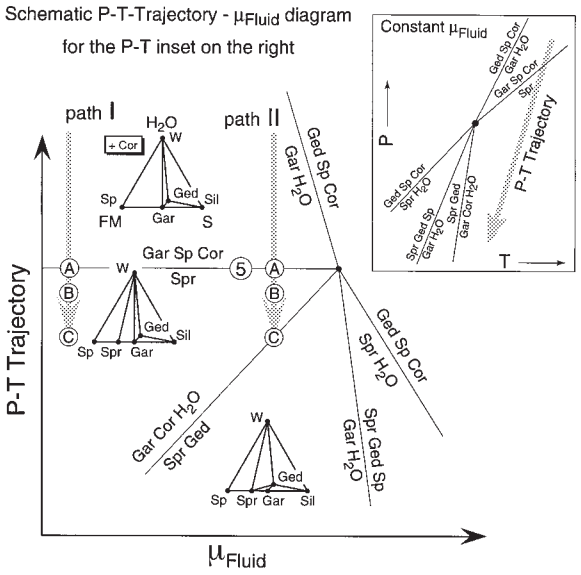

Fig. 9. A schematic *P–T*-path vs μ_{Fluid} diagram that illustrates the manner in which fluid could stabilize gedrite (Ged) during the formation of sapphirine (Spr) coronas at the Munwatte locality. Ternary diagrams are Cor projections onto an FeO + MgO (FM)–SiO_2 (S)–H_2O plane. Arrows are hypothetical paths followed by two identical Gar + Cor + Sp assemblages, one with relatively less (path I) and one with relatively more (path II) fluid present. Opx, orthopyroxene; Sp, spinel; Gar, garnet; Cor, corundum; W, H_2O. The '5' enclosed in a circle is the reaction number used in the text and in other figures, and the letters enclosed in a circle are specific points along paths I and II that are discussed in the text.

little H_2O-bearing fluid present (relatively low μ_{Fluid}) and one with more fluid present (relatively higher μ_{Fluid}).

While undergoing decompression and cooling, both bulk compositions would simultaneously encounter the continuous Fe–Mg reaction (5) and sapphirine production would commence in all bulk compositions, regardless of the fluid content (Fig. 9, points A). The sapphirine forms moats that separate garnet from corundum and spinel. This indicates that the reaction boundary was overstepped and diffusion-controlled mineral growth continued at conditions at which Gar + Sp + Cor were metastable, but still present (Fig. 9, points B). As *P–T* conditions changed further and diffusion-controlled sapphirine growth continued, the reaction boundary Gar + Cor = Spr + Ged could locally be encountered where more fluid phase was present in the bulk composition (Fig. 9, path II, point C). It is suggested that most of the fluid that was present was consumed by the gedrite. As the gedrite became entrapped in the sapphirine, the fluid would have been effectively fractionated out of the reactive bulk composition, which would be shifted towards lower μ_{H_2O} (towards point C, path I in Fig. 9). Sapphirine could then continue to form via reaction (5) until the increasing distance between reactants precluded further sapphirine growth, and produced textures that are observed at the Munwatte locality.

Cordierite-bearing assemblages: possible influence of fluids

Although the reactions that were described above provide a reasonably complete description of the textural sequences, some observations remain unexplained. For example, within the same thin section, relict Sil–Opx interfaces (see Fig. 3e) can be found in equal abundance with places where Sil + Opx have reacted to form Spr + Crd symplectites [reaction (12)].

This minor inconsistency may also be explained by the presence of a multicomponent fluid phase, which could have locally stabilized cordierite to higher pressures as a result of the incorporation of H_2O or CO_2 (Newton, 1972; Newton & Wood, 1979). A scenario that explains the observations can be illustrated on a (*P–T*-path)–μ_{Fluid} diagram, where *P–T*-path and μ_{Fluid} represent schematically changes along the *P–T* path and the effects of varying locally the amounts of fluid that are present and the activity of fluid components, respectively. Figure 10 shows the possible effects of variations in cordierite stability (H_2O or CO_2 content) on the continuous reactions for one set of compositions around the univariant curve 10 (Figs 6 and 7a).

The paths in Fig. 10 show the sequence of reactions that could have been crossed for bulk compositions that were essentially identical except for the amounts of fluid that were present. [The *T* paths shown here are schematic. They would actually not be straight lines and their form would depend upon whether the mineral growth is reaction controlled or diffusion controlled. Straight-line paths conform more closely to the diffusion-controlled case, which is suggested by corona-forming reactions. For further and more detailed discussion of these types of diagrams, see Schumacher & Robinson (1987) and Hensen (1988) and the references therein.] Path I represents less fluid and path II more fluid in the local bulk composition. Locally, where more fluid was available, Gar + Sil + Qz assemblages would begin to form cordierite (path II), but Gar + Sil + Qz would be stable in 'drier' parts of the rock (point B, path I, Fig. 10). Likewise, Gar + Qz assemblages would break down to Crd + Opx where fluid is available (point B, path II, Fig. 10), and remain stable (point B, path I, Fig. 10) where it is not. In the 'drier' assemblages, Gar + Qz would break down to Opx + Sil (point C, path I, Fig. 10) followed by cordierite formation in Opx + Sil + Qz assemblages (points C and D, path I, Fig. 10); whereas, in the 'wetter' assemblages cordierite or Crd + Opx would continue to

form via diffusion-controlled mineral growth (points C and D, path II, Fig. 10) until some combination of factors such as depletion of the fluid phase, reaction kinetics and length of diffusion gradients ended further mineral growth. Essentially, local access and availability of fluid would determine which of the possible product assemblages would develop in the coronas, and all of the assemblages are consistent with the rocks following a single *P–T* trajectory.

THERMOBAROMETRY

Equilibrium *P* and *T* of some key assemblages were estimated using the TWEEQU method (e.g. Berman, 1991; Lieberman & Petrakakis, 1991) with the GEØ-CALC software (Berman, 1988; Brown *et al.*, 1988). Figure 11 shows the equilibria and the phase components that were involved in obtaining *P–T* estimates. The assemblages Opx + Cor + Gar [reaction (1)] and Opx + Sil + Gar + Qz + Plg indicate similar *P–T* conditions in both the Cor-bearing samples (Munwatte) and Qz-bearing samples (Hakurutale) at the end of the garnet-forming stage (Fig. 11a and b), and both give a *P* of ~9–9·2 kbar at ~830°C. Assemblage Gar + Qz + Opx + Crd [reaction (11)], formed during the corona stage, gives lower *P* of ~7·5 kbar at just over 800°C (Fig. 11c). Together, these data suggest that near-isothermal decompression from ~9 kbar to 7·5 kbar occurred at temperatures of ~830–810°C (summarized in Fig. 11d). This decompression path is consistent with the retrograde part of the qualitative *P–T* path (Figs 6, 7a and 8a), and the location of the *P–T* path relative to the equilibria calculated in Figs 7b and 8b.

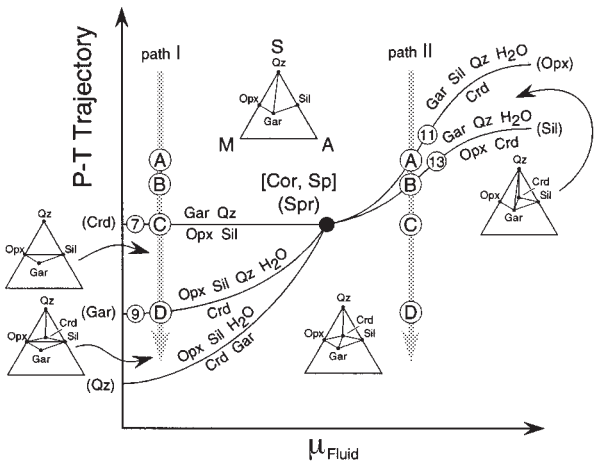

Fig. 10. A schematic *P–T*-path vs μ_{Fluid} diagram that shows the effects that variations of cordierite (Crd) stability as a result of fluid could have on the corona-forming reactions at the Hakurutale locality. Ternary diagrams are FeO + MgO (M)–Al_2O_3 (A)–SiO_2 (S) ternaries. Arrows are hypothetical paths followed by two identical Gar + Cor + Sp assemblages, one with relatively less (path I) and one with relatively more (path II) fluid present. Crd, cordierite; Spr, sapphirine; Opx, orthopyroxene; Gar, garnet; Qz, quartz. The numbers enclosed in a circle are the reaction numbers used in the text and in other figures, and the letters enclosed in a circle are specific points along paths I and II that are discussed in the text.

DISCUSSION AND CONCLUSIONS

Sapphirine + quartz assemblages

In our samples no textural evidence exists for the stability of sapphirine and quartz at any stage, in contrast to otherwise similar samples described by Droop & Bucher-Nurminen (1984) and Bertrand *et al.* (1992). Although both minerals appear together in some thin sections from the Hakurutale outcrop, they appear to be present in separate sub-assemblages. Consequently, we cannot corroborate the inferred stable occurrence of sapphirine + quartz reported by Osanai (1989) in the first description of sapphirine from Sri Lanka (localities are in the same general area as those studied here; see Fig. 1). Those workers also described magnetite and haematite in their samples, which suggests higher ferric iron contents, but the relation of these oxide phases to the sapphirine, if any, is not clear. Nevertheless, this observation may support the contention of Hensen (1986) and Powell & Sandiford (1988) that the stability field of the assemblage sapphirine + quartz expands in bulk compositions that are rich in ferric iron.

Implications of the cordierite-forming reactions in fluid-poor rocks

We suggested earlier that cordierite growth was promoted by the local presence of a fluid phase, and that this feature explains the development in close proximity of different reaction products (e.g. Crd + Opx vs Opx + Sil) from the same sets of reactants (e.g. Gar + Qz). This process has additional implications, because, in fluid-poor rocks such as these, the onset of cordierite formation would incorporate H_2O. As these corona-forming reactions are diffusion controlled, their progress is naturally highly dependent on rates of diffusion, which are enhanced by the presence of H_2O as well as temperature. Essentially, the cordierite-forming reactions sow the seeds of their own extinction; as the cordierite forms and H_2O is incorporated, the reaction kinetics would slow down and the reaction progress would eventually halt.

P–T trajectory

Sapphirine-bearing and associated granulites in Sri Lanka followed a roughly 'clockwise' *P–T* path that can be

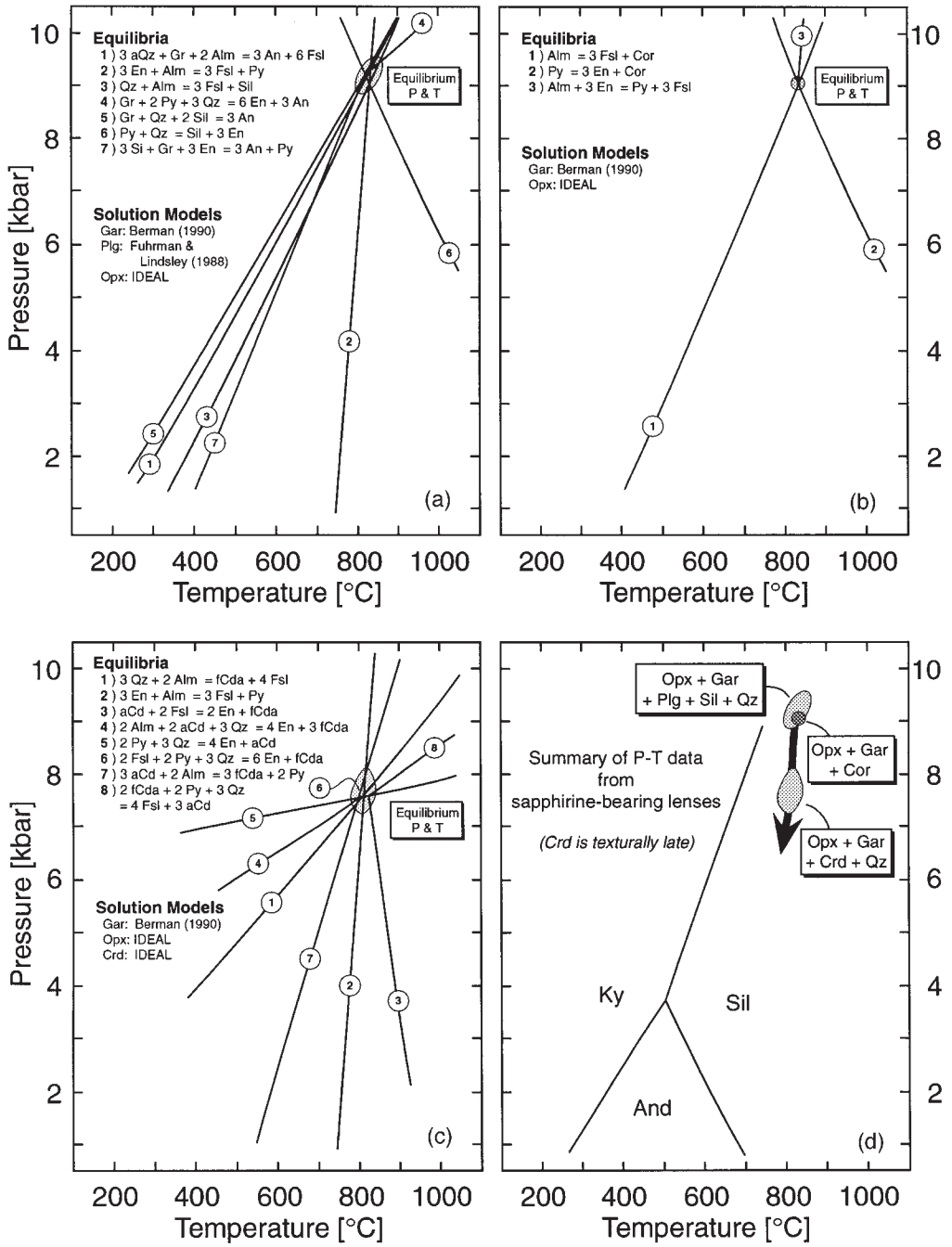

Fig. 11. *P–T* conditions derived for various assemblages using the TWEEQU method and GEØ-CALC software (Berman, 1991; Lieberman & Petrakakis, 1991). Crd, cordierite solid solution; aCd, anhydrous Mg-cordierite; fCda, anhydrous Fe-cordierite; Opx, orthopyroxene solid solution; En, enstatite; Fsl, orthoferrosilite; Gar, garnet solid solution; Py, pyrope; Alm, almandine; Gr, grossular; Plg, plagioclase solid solution; An, anorthite; Sil, sillimanite; aQz, α quartz; Cor, corundum. (a) *P–T* estimates for the assemblage Gar + Qz + Opx + Sil + Plg (Hakurutale) that give ~9·2 kbar, 820°C. (b) *P–T* estimates for the assemblage Opx + Cor + Gar (Munwatte) that give ~9·0 kbar, 830°C. (c) *P–T* estimates for the assemblage Gar + Qz + Opx + Crd (Hakurutale) that give 7·6 kbar, 800°C. (d) A summary of data from parts (a)–(c) and partial *P–T* path (arrow).

divided into two main phases. The early, prograde part of the path is characterized by garnet formation. During the post-peak part of the trajectory, spectacular corona-type textures developed. In the varieties (sillimanite- and quartz-bearing) that are richer in SiO_2, cordierite is commonly formed whereas garnet is generally consumed.

On the basis of both the slopes of reactions that were inferred from the textures in thin section and *P–T* estimates, the corona–cordierite formation records near-isothermal decompression beginning at ~830°C and 9 kbar and continuing to at least ~810°C and 7·5 kbar. These *P–T* estimates are in good agreement with those on similar rocks from the Alps (Droop & Bucher-Nurminen, 1984).

The evidence from sapphirine-bearing granulites supports the interpretation that the sequence kyanite followed by sillimanite followed by andalusite in metapelites formed during a single metamorphic cycle evolving along an essentially clockwise *P–T* path (Hiroi *et al.*, 1990, 1994; Raase & Schenk, 1994; see also Kriegsman, 1996). In contrast in the metamorphosed basic rocks, growth of garnet + quartz ± clinopyroxene from plagioclase + orthopyroxene occurs at high temperature, and subsequently garnet breaks down to a new generation of orthopyroxene + plagioclase. This has been interpreted as evidence of near-isobaric cooling at high pressures followed by decompression (Schenk *et al.*, 1988; Schumacher *et al.*, 1990; Schumacher & Faulhaber, 1994). Support for this interpretation comes from high temperatures recorded in exsolved coexisting pyroxenes (Schenk *et al.*, 1988).

The data for the decompression stage of the *P–T* trajectory both from this study and the work on the metamorphosed basic rocks are in reasonable agreement (Schumacher & Faulhaber, 1994). However, data for the orientation of the *P–T* trajectory just before the decompression from the same two rock types appear to be slightly contradictory (Fig. 12). At present, it is not possible to resolve conclusively this apparent contradiction. One possible explanation is that the highest granulite-facies temperatures (>900°C), although widely distributed, were not reached everywhere. The source of the high-temperature thermal anomaly is not well understood. For example, the high temperatures could be due, in part, to the influence of synmetamorphic intrusive bodies. Such intrusives could have contributed to the overall heating of the terrane, but they would have also caused local heating and cooling spikes. This could have led to the near-isobaric heating and cooling locally, which would not necessarily be seen everywhere in the terrane. Unfortunately, intense weathering of large areas of the terrane precludes a complete understanding of the field relations at many localities.

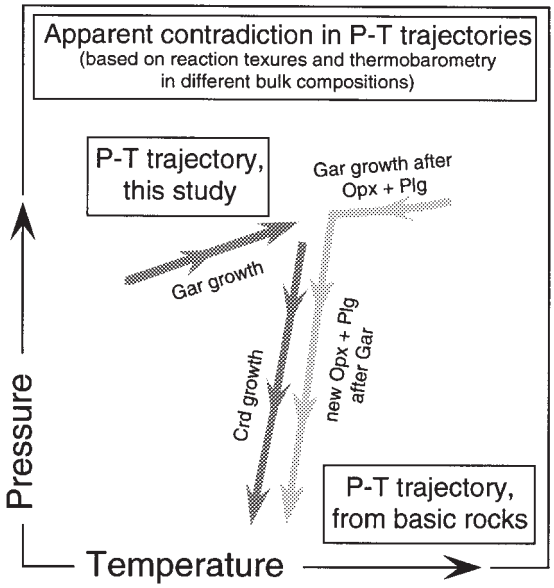

Fig. 12. Comparison of the *P–T* trajectory of this study and part of the trajectory from the work of Schenk *et al.* (1988), Schumacher *et al.* (1990) and Schumacher & Faulhaber (1994).

ACKNOWLEDGEMENTS

This work was supported by a German Science Foundation (DFG) grant and by travel grants from the Dutch 'Dr. Schürmannfonds' to L.M.K. Piet Thijssen and Timo Nijland are thanked for their help to L.M.K. during the early stages of this project. Valuable discussions with all members of the German–Sri Lanka Consortium have been indispensable. J.C.S. would, in particular, like to thank Renate Schumacher, Volker Schenk and Peter Raase, members of the German–Sri Lanka Consortium, whose ideas and years of intensive work on the geology and petrology of Sri Lanka contributed greatly to the present project. Constructive reviews of this manuscript were generously provided by Kurt Bucher and Giles Droop.

REFERENCES

Baur, N., Kröner, A., Todt, W., Liew, T. C. & Hofmann, A. W. (1991). U–Pb isotopic systematics of zircons from prograde and retrograde transition zones in high-grade orthogneisses, Sri Lanka. *Journal of Geology* **99,** 527–545.

Berger, A. R. & Jayasinghe, N. R. (1976). Precambrian structure and chronology in the Highland Series of Sri Lanka. *Precambrian Research* **3,** 559–576.

Berman, R. G. (1988). Internally-consistent thermodynamic data for minerals in the system Na_2O–K_2O–CaO–MgO–FeO–Fe_2O_3–Al_2O_3–SiO_2–TiO_2–H_2O–CO_2. *Journal of Petrology* **29,** 445–522.

Berman, R. G. (1990). Mixing properties of Ca–Mg–Fe–Mn garnets. *American Mineralogist* **75,** 328–344.

Berman, R. G. (1991). Thermometry using multi-equilibrium calculations: a new technique, with petrological applications. *Canadian Mineralogist* **29,** 833–855.

Bertrand, P., Ellis, D. J. & Green, D. H. (1991). The stability of sapphirine–quartz and hypersthene–sillimanite–quartz assemblages: an experimental investigation in the system FeO–MgO–Al_2O_3–SiO_2 under H_2O, H_2O–CO_2 and CO_2 conditions. *Contributions to Mineralogy and Petrology* **108,** 55–71.

Bertrand, P., Ouzegane, K. & Kienast, J. R. (1992). *P–T–X* relationships in the Precambrian Al–Mg–rich granulites from In Ouzzal, Hoggar, Algeria. *Journal of Metamorphic Geology* **10,** 17–31.

Brown, T. H., Berman, R. G. & Perkins, E. H. (1988). GEØ-CALC: software package for the calculation and display of pressure–temperature–composition phase diagrams using an IBM or compatible personal computer. *Computers and Geosciences* **14,** 279–289.

Caporuscio, F. A. & Morse, S. A. (1978). Occurrence of sapphirine plus quartz at Peeskill, New York. *American Journal of Science* **278,** 1334–1342.

Connolly, J. A. D. (1990). Multivariable phase diagrams: an algorithm based on generalized thermodynamics. *American Journal of Science* **290,** 666–718.

Cooray, P. G. (1994). The Precambrian of Sri Lanka: a historical review. *Precambrian Research* **66,** 3–18.

Droop, G. T. R. (1987). A general equation for estimating Fe^{3+} concentrations in ferromagnesian silicates and oxides from microprobe analyses using stoichiometric criteria. *Mineralogical Magazine* **51,** 431–435.

Droop, G. T. R. (1989). Reaction history of garnet–sapphirine granulites and conditions of Archaean high-pressure granulite-facies metamorphism in the central Limpopo Mobile Belt, Zimbabwe. *Journal of Metamorphic Geology* **7,** 383–403.

Droop, G. T. R. & Bucher-Nurminen, K. (1984). Reaction textures and metamorphic evolution of sapphirine-bearing granulites of the Gruf Complex, Italian Central Alps. *Journal of Petrology* **25,** 766–803.

Faulhaber, S. & Raith, M. (1991). Geothermometry and geobarometry of high-grade rocks a case study on garnet–pyroxene granulites in southern Sri Lanka. *Mineralogical Magazine* **55,** 17–40.

Goscombe, B. (1992). Silica-undersaturated sapphirine, spinel and kornerupine granulite facies rocks, NE Strangways Range, Central Australia. *Journal of Metamorphic Geology* **10,** 181–201.

Harley, S. L. & Fitzsimons, I. C. W. (1991). Pressure–temperature evolution of metapelitic granulites in a polymetamorphic terrane: Raurer Group, East Antarctica. *Journal of Metamorphic Geology* **9,** 231–243.

Hensen, B. J. (1971). Theoretical phase relations involving cordierite and garnet in the system MgO–FeO–Al_2O_3–SiO_2. *Contributions to Mineralogy and Petrology* **33,** 191–214.

Hensen, B. J. (1986). Theoretical phase relations involving cordierite and garnet revisited; the influence of oxygen fugacity on the stability of sapphirine and spinel in the system Mg–Fe–Al–Si–O. *Contributions to Mineralogy and Petrology* **92,** 362–367.

Hensen, B. J. (1987). *P,T*-grids for silica-undersaturated granulites in the systems MAS(n + 4) and FMAS(n + 3); tools for the derivation of *P–T* paths of metamorphism. *Journal of Metamorphic Geology* **5,** 255–271.

Hensen, B. J. (1988). Chemical potential diagrams and chemographic projections: applications to sapphirine-granulites from Kiranur and Ganguvarpatti, Tamil Nadu: evidence for rapid uplift in part of the South Indian Shield? *Neues Jahrbuch für Mineralogie, Abhandlungen* **158,** 193–210.

Hensen, B. J. & Harley, S. L. (1990). Graphical analysis of *P–T–X* relations in granulite facies metapelites. In: Brown, M. & Ashworth, J. R. (eds) *High-Grade Metamorphism and Crustal Anatexis*. London: Allan and Unwin, pp. 19–55.

Hiroi, Y., Asami, M., Cooray, P. G., Fernando, M. R. D., Jayatileke, J. M. S., Kagami, H., Mathavan, V., Matsueda, H., Motoyoshi, Y., Ogo, Y., Osanai, Y., Owada, M., Perera, L. R. K., Prame, K. B. N., Ranasinghe, N. S., Shiraishi, K., Vitanage, P. W. & Yoshida, M. (1990). Arrested charnockitisation in Sri Lanka field and petrographical evidence for low-pressure conditions. In: Hiroi, Y. & Motoyoshi, Y. (eds) *Study of Geologic Correlation between Sri Lanka and Antarctica (1988–1989)*. Chiba, Japan: Chiba University, pp. 1–18.

Hiroi, Y., Ogo, Y. & Namba, K. (1994). Evidence for prograde metamorphic evolution of Sri Lankan pelitic granulites, and implications for the development of continental crust. *Precambrian Research* **66,** 245–263.

Holland, T. J. B. (1989). Dependence of entropy on volume for silicate and oxide minerals: a review and predictive model. *American Mineralogist* **74,** 5–13.

Hölzl, S., Hofmann, A. W., Todt, W. & Köhler, H. (1994). U–Pb geochronology of the Sri Lankan basement. *Precambrian Research* **66,** 123–149.

Korzhinskii, D. S. (1959). *Physiochemical Basis of the Analysis of the Petrogenesis of Minerals*. New York: Consultants Bureau, 142 pp.

Kriegsman, L. M. (1991*a*). Sapphirine-bearing granulites from central Sri Lanka—outcrop description and mineral chemistry. In: Kröner, A. (ed.) *The Crystalline Crust of Sri Lanka, Part 1, Summary of Research of the German–Sri Lankan Consortium. Geological Survey Department of Sri Lanka, Professional Paper* **5,** 178–187.

Kriegsman, L. M. (1991*b*). The Munwatte outcrop. In: Voll, G. & Kleinschrodt, R. (eds) *The Crystalline Crust of Sri Lanka, Part II, Excursion Guide for Geological Field Trip in Sri Lanka. Geological Survey Department of Sri Lanka, Professional Paper* **6,** 31–34.

Kriegsman, L. M. (1994). Evidence for a fold nappe in the high grade basement of central Sri Lanka: terrane assembly in Pan-African lower crust. *Precambrian Research* **66,** 57–76.

Kriegsman, L. M. (1996). Divariant and trivariant reaction line slopes in FMAS and CFMAS: theory and applications. *Contributions to Mineralogy and Petrology* **126,** 38–50.

Kröner, A. (1991). African linkage of Precambrian Sri Lanka. *Geologische Rundschau* **80,** 429–440.

Lal, R. K., Ackermand, D., Raase, P. & Seifert, F. (1984). Sapphirine bearing assemblages from Kiranur, Southern India. A study of chemographic relations in the Na_2O–FeO–MgO–Al_2O_3–SiO_2–H_2O system. *Neues Jahrbuch für Mineralogie, Abhandlungen* **150,** 121–152.

Lieberman, J. & Petrakakis, K. (1991). TWEEQU thermobarometry: analysis of uncertainties and applications to granulites from western Alaska and Austria. *Canadian Mineralogist* **29,** 857–887.

Massonne, H.-J. (1992). Thermodynamische Eigenschaften von Phasen des Systems MgO–Al_2O_3–SiO_2–H_2O (MASH) unter besonder Berücksichtigung von Mischkristallreihen. *Beihefte zur European Journal of Mineralogy* **4,** 186.

Milisenda, C. C., Liew, T. C., Hofmann, A. W. & Kröner, A. (1988). Isotopic mapping of age provinces in Precambrian high-grade terrains, Sri Lanka. *Journal of Geology* **96,** 608–615.

Newton, R. C. (1972). An experimental determination of the high pressure stability limits of magnesian cordierite under wet and dry conditions. *Journal of Geology* **80,** 398–420.

Newton, R. C. & Wood, B. J. (1979). Thermodynamics of water in cordierite and some petrologic consequences of cordierite as a hydrous phase. *Contributions to Mineralogy and Petrology* **68,** 391–405.

Osanai, Y. (1989). A preliminary report on sapphirine/kornerupine granulite from Highland Series, Sri Lanka (extended abstract). *Seminar on Recent Advances in Precambrian Geology of Sri Lanka.*

Powell, R. & Sandiford, M. (1988). Sapphirine and spinel phase relationships in the system FeO–MgO–Al_2O_3–SiO_2–TiO_2–O_2 with presence of quartz and hypersthene. *Contributions to Mineralogy and Petrology* **98,** 64–71.

Prame, W. K. B. N. (1991*a*). Metamorphism and nature of granulite-facies crust in southwestern Sri Lanka: characterization by pelitic/psammopelitic rocks and associated granulites. In: Kröner, A. (ed.) *The Crystalline Crust of Sri Lanka, Part I, Summary of Research of the*

German–Sri Lankan Consortium. Geological Survey Department of Sri Lanka, Professional Paper **5,** 188–199.

Prame, W. K. B. N. (1991*b*). Petrology of the Kataragama Complex, Sri Lanka: evidence for high granulite facies metamorphism and subsequent isobaric cooling. In: Kröner, A. (ed.) *The Crystalline Crust of Sri Lanka, Part I, Summary of Research of the German–Sri Lankan Consortium. Geological Survey Department of Sri Lanka, Professional Paper* **5,** 200–224.

Raase, P. & Schenk, V. (1994). Petrology of granulite-facies metapelites of the Highland Complex, Sri Lanka: implications for the metamorphic zonation and the *P–T* path. *Precambrian Research* **66,** 265–294.

Regan, C. P. & Stout, J. H. (1992). Alternative FMAS phase diagrams for granulite terranes based on concept parity mapping. *EOS Transactions, American Geophysical Union* **73,** 327.

Robinson, P. & Jaffe, H. W. (1969). Aluminous enclaves in gedrite–cordierite gneiss from southwestern New Hampshire. *American Journal of Science* **267,** 389–421.

Robinson, P., Spear, F. S., Schumacher, J. C., Laird, J., Klein, C., Evans, B. W. & Doolan, B. L. (1982). Phase relations of metamorphic amphiboles: natural occurrence and theory. In: Veblen, D. R. & Ribbe, P. H. (eds) *Amphiboles: Petrology and Experimental Phase Relation. Mineralogical Society of America, Reviews in Mineralogy* **9B,** 1–227.

Sandiford, M., Powell, R., Martin, S. F. & Perera, L. R. K. (1988). Thermal and baric evolution of garnet granulites from Sri Lanka. *Journal of Metamorphic Geology* **6,** 351–364.

Schenk, V., Raase, P. & Schumacher, R. (1988). Very high temperatures and isobaric cooling before tectonic uplift in the Highland Series of Sri Lanka. *Terra Cognita* **8,** 265.

Schreyer, W. & Seifert, F. (1969). Compatibility relations of the aluminum silicates in the system $MgO–Al_2O_3–SiO_2–H_2O$ and $K_2O–MgO–Al_2O_3–SiO_2–H_2O$ at high pressures. *American Journal of Science* **267,** 371–388.

Schumacher, J. C. (1991). Empirical ferric iron corrections of electron microprobe mineral analyses: necessity, assumptions, and effects on some geothermometers and geobarometers. *Mineralogical Magazine* **55,** 3–18.

Schumacher, J. C. & Robinson, P. (1987). Mineral chemistry and metasomatic growth of aluminous enclaves in gedrite–cordierite gneiss, southwestern New Hampshire. *Journal of Petrology* **28,** 1033–1073.

Schumacher, R. & Faulhaber, S. (1994). Summary and discussion of *P–T* estimates from garnet–pyroxene–plagioclase–quartz-bearing granulite-facies rocks from Sri Lanka. *Precambrian Research* **66,** 295–308.

Schumacher, R., Schenk, V., Raase, P. & Vitanage, P. W. (1990). Granulite facies metamorphism of metabasic and intermediate rocks in the Highland Series of Sri Lanka. In: Brown, M. & Ashworth, J. R. (eds) *High-grade Metamorphism and Crustal Anatexis*. London: Allan and Unwin, pp. 235–271.

Seifert, F., Ackermand, D. & Czank, M. (1992). A coherent orthopyroxene exsolution from sapphirine. *Zeitschrift für Kristallographie* **199**(1–2), 99–111.

Selkregg, K. R. & Bloss, F. D. (1980). Cordierites: compositional controls of Δ, cell parameters, and optical properties. *American Mineralogist* **65,** 522–533.

Spear, F. S. (1982). Phase equilibria of amphibolites from the Post Pond Volcanics, Mt. Cube Quadrangle, Vermont. *Journal of Petrology* **23,** 383–427.

Vielzeuf, D. (1983). The spinel and quartz associations in high grade xenoliths from Tallante (S.E. Spain) and their potential use in geothermometry and barometry. *Contributions to Mineraology and Petrology* **82,** 301–311.

Waters, D. J. (1986). Metamorphic history of sapphirine bearing and related Magnesian gneisses from Namaqualand, South Africa. *Journal of Petrology* **27,** 541–565.